Deschloroclozapine, a potent and selective chemogenetic actuator enables rapid neuronal and behavioral modulations in mice and monkeys

Yuji Nagai [1,10], Naohisa Miyakawa [1,10], Hiroyuki Takuwa[1], Yukiko Hori[1], Kei Oyama[1], Bin Ji[1], Manami Takahashi[1], Xi-Ping Huang[2,3], Samuel T. Slocum [2], Jeffrey F. DiBerto[2], Yan Xiong[4], Takuya Urushihata[1], Toshiyuki Hirabayashi[1], Atsushi Fujimoto [1], Koki Mimura[1], Justin G. English [2], Jing Liu[4], Ken-ichi Inoue [5,6], Katsushi Kumata[7], Chie Seki[1], Maiko Ono[1], Masafumi Shimojo[1], Ming-Rong Zhang[7], Yutaka Tomita[8], Jin Nakahara[8], Tetsuya Suhara[1], Masahiko Takada[5], Makoto Higuchi[1], Jian Jin [4], Bryan L. Roth [2,3,9 ✉] and Takafumi Minamimoto [1✉]

The chemogenetic technology designer receptors exclusively activated by designer drugs (DREADDs) afford remotely reversible control of cellular signaling, neuronal activity and behavior. Although the combination of muscarinic-based DREADDs with clozapine-*N*-oxide (CNO) has been widely used, sluggish kinetics, metabolic liabilities and potential off-target effects of CNO represent areas for improvement. Here, we provide a new high-affinity and selective agonist deschloroclozapine (DCZ) for muscarinic-based DREADDs. Positron emission tomography revealed that DCZ selectively bound to and occupied DREADDs in both mice and monkeys. Systemic delivery of low doses of DCZ (1 or 3 µg per kg) enhanced neuronal activity via hM3Dq within minutes in mice and monkeys. Intramuscular injections of DCZ (100 µg per kg) reversibly induced spatial working memory deficits in monkeys expressing hM4Di in the prefrontal cortex. DCZ represents a potent, selective, metabolically stable and fast-acting DREADD agonist with utility in both mice and nonhuman primates for a variety of applications.

The chemogenetic technology DREADD affords a minimally invasive means to reversibly and remotely control the activity of DREADD-expressing cells through the systemic delivery of DREADD ligands[1]. Several DREADDs exist, derived from muscarinic or κ-opioid receptors[1,2], and they have been widely adopted for neuroscience research[3]. Muscarinic receptor DREADDs are the most widely used and can be activated by CNO (Fig. 1d, right). Activation of a modified human M3 muscarinic receptor (hM3Dq) enhances neuronal activity, while a modified M4 receptor (hM4Di) silences it. CNO-activated DREADDs have been successfully applied in a variety of in vitro and in vivo contexts, including in nonhuman primate studies to modify neural network activity[4] and behavior[5–7].

Since CNO has modest brain permeability, relatively large systemic doses may be required for DREADD activation. Moreover, CNO can be metabolized to clozapine (Fig. 1a, right), which is a potent, brain-permeable DREADD agonist[1,8]. CNO metabolism to clozapine is non-negligible in rodents[8,9] and in monkeys[10]. In addition to activating DREADDs, clozapine potently binds to many endogenous receptors and transporters[11]; thus, CNO or clozapine can produce confounding off-target side effects. Although alternative DREADD agonists, such as compound 21 (C21) (Fig. 1d, left) and perlapine[12,13], have been recently developed, they require relatively large systemic doses to activate DREADDs in vivo and may have off-target actions[13]. Given the broad utility and popularity of muscarinic-based DREADDs, the development of a selective, high-affinity, metabolically stable and brain-penetrable DREADD agonist is important.

Here, we identified a suitable DREADD agonist that we have named DCZ (11-(4-methyl-1-piperazinyl)-5*H*-dibenzo(*b*,*e*)(1,4) diazepine) (Fig. 1a, left), which is derived from our previous studies of DREADD ligands for muscarinic-based DREADDs[12]. We became aware of DCZ as it had been previously reported to have substantially lower affinity for dopaminergic (D1 and D2) and serotonergic (5-HT$_{2A}$ and 5-HT$_{2C}$) receptors than clozapine[14]. We determined that DCZ has 100-fold improved affinity and greater agonist potency for hM3Dq and hM4Di relative to CNO or C21, with reduced off-target binding compared to clozapine in vitro. Using positron emission tomography (PET), we demonstrate that DCZ is rapidly brain penetrable, is apparently selective and that doses for

---

[1]Department of Functional Brain Imaging, National Institute of Radiological Sciences, National Institutes for Quantum and Radiological Science and Technology, Chiba, Japan. [2]Department of Pharmacology, University of North Carolina at Chapel Hill School of Medicine, Chapel Hill, NC, USA. [3]Division of Chemical Biology and Medicinal Chemistry, Eshelman School of Pharmacy, University of North Carolina at Chapel Hill, Chapel Hill, NC, USA. [4]Mount Sinai Center for Therapeutics Discovery, Departments of Pharmacological Sciences and Oncological Sciences, Tisch Cancer Institute, Icahn School of Medicine at Mount Sinai, New York, NY, USA. [5]Systems Neuroscience Section, Primate Research Institute, Kyoto University, Inuyama, Japan. [6]PRESTO, Japan Science and Technology Agency, Kawaguchi, Saitama, Japan. [7]Department of Radiopharmaceuticals Development, National Institute of Radiological Sciences, National Institutes for Quantum and Radiological Science and Technology, Chiba, Japan. [8]Department of Neurology, Keio University School of Medicine, Tokyo, Japan. [9]National Institute of Mental Health Psychoactive Drug Screening Program (NIMH PDSP), Department of Pharmacology, University of North Carolina at Chapel Hill Medical School, Chapel Hill, NC, USA. [10]These authors contributed equally: Yuji Nagai and Naohisa Miyakawa.
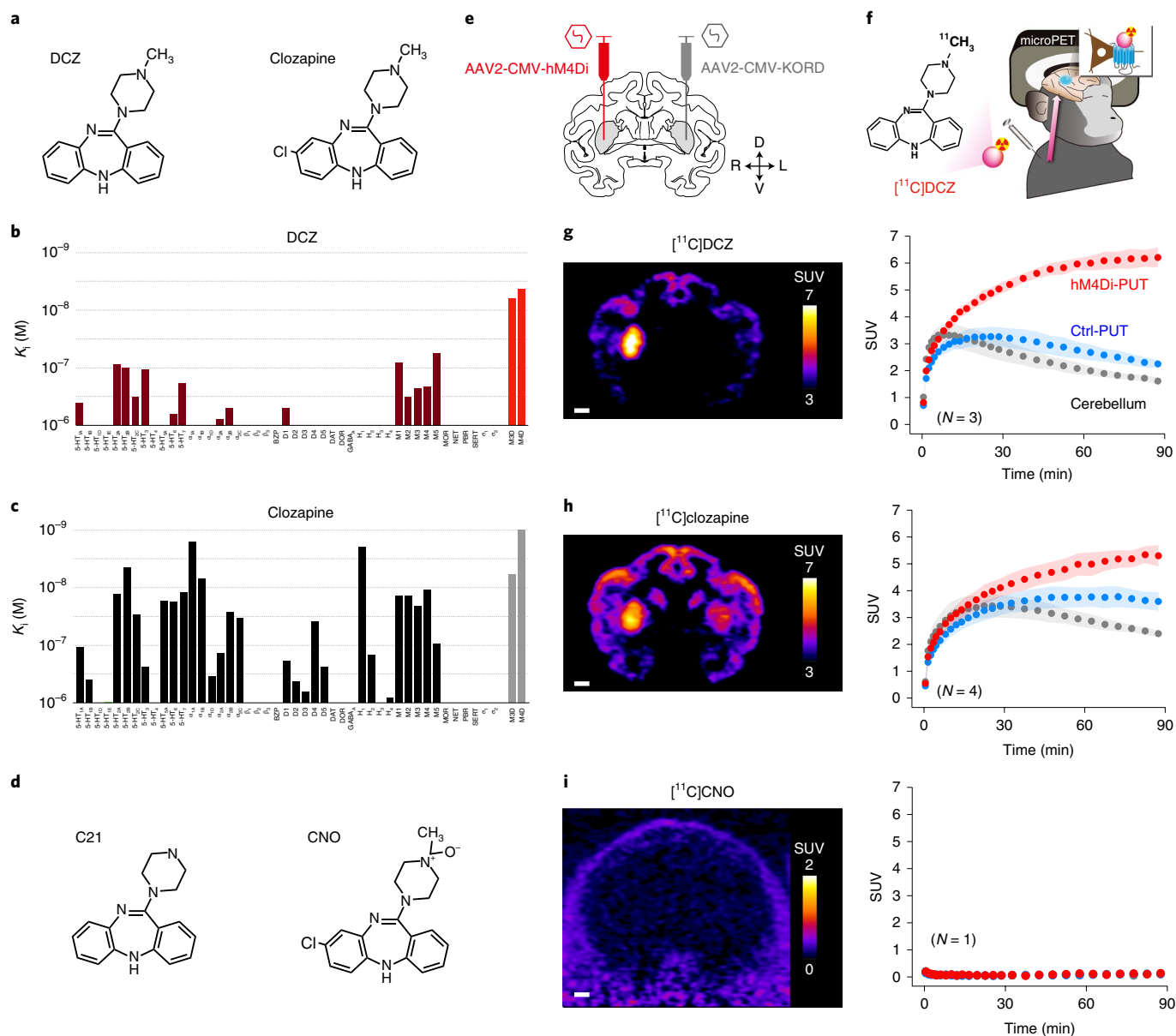✉e-mail: bryan_roth@med.unc.edu; minamimoto.takafumi@qst.go.jp

Fig. 1 | DCZ selectively binds to DREADDs. a, Chemical structure of DCZ and clozapine. **b,c**, Binding affinities of DCZ and clozapine to DREADDs and endogenous receptors, channels and transporters. K_i values are the average of at least three triplicate experiments with standard deviation values that are threefold less than the average. The values are also shown in Table 1 and Supplementary Table 1. **d**, Chemical structure of C21 and CNO. **e**, Illustration of the location of viral vector injections. AAV2-CMV-hM4Di and AAV2-CMV-KORD (as control) were injected into the right and left putamen, respectively. D, dorsal; L, left; R, right; V, ventral. **f**, Illustration of in vivo PET imaging with [^{11}C]DCZ in monkeys. **g–i**, Representative PET imaging data obtained from monkey 209. **g**, Left: coronal section of a PET image of [^{11}C]DCZ SUVs (regional radioactivity (Bq cm^{-3}) × body weight (g)/injected radioactivity (Bq)) between 30 and 90 min from injection. Right: the time course of regional uptake (mean ± s.d., $N = 3$ scans) of [^{11}C]DCZ at the hM4Di-expression region in the putamen (hM4Di-PUT), a control region in the contralateral putamen (Ctrl-PUT), and the cerebellum. **h**, Same as **g** but with [^{11}C]clozapine ($N = 4$). **i**, Same as **g** but with [^{11}C]CNO ($N = 1$). Scale bars, 5 mm.

DREADD occupancy are 20-fold and 60-fold lower than CNO and C21, respectively. Finally, we demonstrate that DCZ is capable of rapidly (<10 min post-injection) activating hM3Dq and hM4Di in both mice and monkeys without discernible off-target action. Thus, DCZ represents a potent and selective chemogenetic actuator for muscarinic-based DREADDs in mice and primates in a variety of in vitro and in vivo contexts with high translational potential.

Results

DCZ selectively binds to DREADDs in vitro and in vivo. We first assessed the binding affinities of DCZ to hM3Dq and hM4Di and

compared them to those of clozapine, CNO and C21 using competition binding assays with [^{3}H]quinuclidinyl benzilate (QNB) on HEK293T cells. DCZ had nanomolar affinity for [^{3}H]QNB-labeled hM3Dq and hM4Di (inhibition constant (K_i) values of 6.3 nM for hM3Dq and 4.2 nM for hM4Di), which was comparable to clozapine ($^{hM3Dq}K_i = 5.9$ nM, $^{hM4Di}K_i = 0.89$). CNO and C21 were about 100-fold and 50-fold weaker, respectively (CNO: $^{hM3Dq}K_i = 680$ nM, $^{hM4Di}K_i = 360$ nM; C21: $^{hM3Dq}K_i = 850$ nM, $^{hM4Di}K_i = 180$ nM) (Table 1). Unlike clozapine (Fig. 1c; Supplementary Table 1), DCZ had negligible affinities for a large number of tested G protein-coupled receptors (GPCRs), ion channels and transporters (K_i values of >100 nM)

Table 1 | Binding affinities of DCZ, clozapine and CNO to DREADDs and native muscarinic receptors

Compound	Mean values	hM3Dq	hM3	hM4Di	hM4
DCZ	K_i (nM)	6.3	230	4.2	210
	pK_i (±s.e.m)	8.20 (±0.15)	6.63 (±0.06)	8.38 (±0.27)	6.68 (±0.04)
Clozapine	K_i (nM)	5.9	21	0.89	10
	pK_i (±s.e.m)	8.23 (±0.26)	7.69 (±0.14)	9.05 (±0.13)	7.98 (±0.10)
CNO	K_i (nM)	680	2,600	360	3,700
	pK_i (±s.e.m)	6.17 (±0.07)	5.59 (±0.06)	6.44 (±0.03)	5.43 (±0.18)
C21	K_i (nM)	850	270	178[a]	3,631[a]
	pK_i (±s.e.m)	6.07 (±0.06)	6.57 (±0.15)	6.75 (±0.26)	5.44 (±0.11)

The average of at least three duplicate experiments with standard deviation values that are threefold less than average are shown. [a]Data from Thompson et al.[13]. Radioligand binding assays were performed with QNB on HEK293T cells. The average [^{3}H]QNB concentrations were 0.8 nM for hM3/hM4 and 2.0 nM for hM3Dq/hM4Di.

and relatively low affinities for a few endogenous receptors, including muscarinic acetylcholine ($^{hM1}K_i = 83$ nM, $^{hM5}K_i = 55$ nM) and serotonin receptors ($^{5-HT}_{2A}K_i = 87$ nM) (Fig. 1b; Supplementary Table 1), which represents at least an eightfold antagonist binding selectivity for muscarinic DREADDs over its most potent endogenous targets.

We next examined whether DCZ enters the brain and binds to DREADDs in vivo. Here, we performed PET with radiolabeled DCZ ([^{11}C]DCZ) in two monkeys (see Supplementary Table 2 for a summary of the monkeys used in these experiments), which had received an adeno-associated virus type 2 vector (AAV2-CMV-hM4Di) injection that resulted in neuron-specific expression of hM4Di[6] in the right putamen. An AAV2 control vector carrying the κ-opioid-based DREADD (AAV2-CMV-KORD) was injected into the left putamen (Fig. 1e) as it does not bind DCZ (not shown)[2]. Six weeks later, when stable expression is predicted[6], the monkeys were scanned via PET after intravenous (i.v.) administration of a microdose of [^{11}C]DCZ (Fig. 1f). The results revealed rapid brain penetrance of [^{11}C]DCZ with high radioactive accumulation in the hM4Di-expressing putamen (standardized radioligand uptake values (SUVs) at 85–90 min of 6.3 ± 0.4 for monkey 209 and 4.5 ± 0.8 for monkey 212 (mean ± s.d.)). Accumulation in the contralateral putamen was insignificant (2.4 ± 0.7 for monkey 209, 1.7 ± 0.3 for monkey 212) (see Fig. 1g for representative findings), which is in agreement with the high selectivity of DCZ for DREADDs in vitro. Low DCZ uptake was visible in surrounding cortical areas, which potentially reflects DCZ binding to endogenous receptors with low affinities. Using a single subject (monkey 209), brain permeability and selectivity of DCZ were then directly compared to clozapine and CNO, two DREADD agonists whose radiolabeled forms were available; C21 radiolabeled with [^{11}C] was unavailable. Consistent with our previous study[6], PET imaging with microdoses of [^{11}C]clozapine showed moderate uptake at the control putamen and cortical areas (Fig. 1h, left), which likely reflects its high binding affinity for many endogenous receptors (Fig. 1c; Supplementary Table 1), and increased uptake at the hM4Di-expressing putamen region, which presumably reflects clozapine binding to hM4Di (Fig. 1h, left). PET imaging with [^{11}C]CNO revealed a low brain signal, which indicates modest brain permeability (Fig. 1i). Indeed, the concentration of [^{11}C]CNO in the entire brain at 30 min was 0.14% of the injected dose, which was >40-fold lower than that of [^{11}C]DCZ or [^{11}C]clozapine (5.9% and 7.0%, respectively).

Dynamic regional radioactivity reflects radioligand localization in the vascular system and brain tissue in the initial phase and ligand binding to tissue in the later phase. Here, the [^{11}C]DCZ signal at the target region continued to increase, nearly reaching a plateau 90 min after radioligand injection, whereas the signal on the contralateral side moderately increased and then rapidly decayed (Fig. 1g, right). These regional differences in radioactivity were abolished by pretreatment with unlabeled DCZ (1 mg per kg, i.v.) (Supplementary Fig. 1a), and therefore reflect displaceable ligand binding. We quantified specific [^{11}C]DCZ binding to tissue using the cerebellum as a reference region, where radioligand kinetics were unchanged by pretreatment (Supplementary Fig. 1a). On the parametric image representing specific binding, BP_{ND} (that is, the binding potential relative to non-displaceable uptake), high [^{11}C]DCZ was localized to the hM4Di-vector-injected side of the putamen, which corresponds to the area where anti-hM4 post-mortem immunolabeling was found (Fig. 2a,b; Supplementary Fig. 2a), thus confirming that [^{11}C]DCZ binds to hM4Di in vivo. In addition, high [^{11}C]DCZ binding was found in the projection target of the putamen—the substantia nigra—reflecting hM4Di expression at the axon terminals as confirmed by immunohistochemistry (Supplementary Fig. 2b).

To verify in vivo DCZ binding to DREADDs in mice, we performed [^{11}C]DCZ PET imaging with a transgenic mouse expressing hM4Di under the control of the neuron-specific *Thy-1* promoter[15]. [^{11}C]DCZ uptake in the striatum and cortex was upregulated in transgenic mice compared with wild-type mice (Supplementary Fig. 1b, left versus center). In the parametric image, high [^{11}C]DCZ binding was observed in the frontal and parietal cortices, hippocampus and striatum, which is consistent with high hM4Di expression (as confirmed by immunofluorescence). In contrast, no discernible binding was seen in wild-type mouse brains (Supplementary Fig. 2c,d), which implies that there is low off-target binding at this dose. Taken together, our PET results suggest that DCZ rapidly enters the brain and selectively binds to hM4Di expressed in both mice and monkeys.

Systemic low-dose DCZ occupies hM4Di DREADD in vivo. In previous chemogenetic studies, a range of systemic CNO doses were used to obtain behavioral effects, which suggests that the required dose may vary according to the target neuronal population, the type of DREADD and the level/localization of expression, among other factors[16]. Similar to most drugs, at pre-saturation, a higher agonist dose affords a stronger chemogenetic effect, but also has greater off-target potential. Although DCZ has lower levels of off-target binding than clozapine, finding the effective and safe dose range for systemic DCZ administration is critical for studies seeking selective
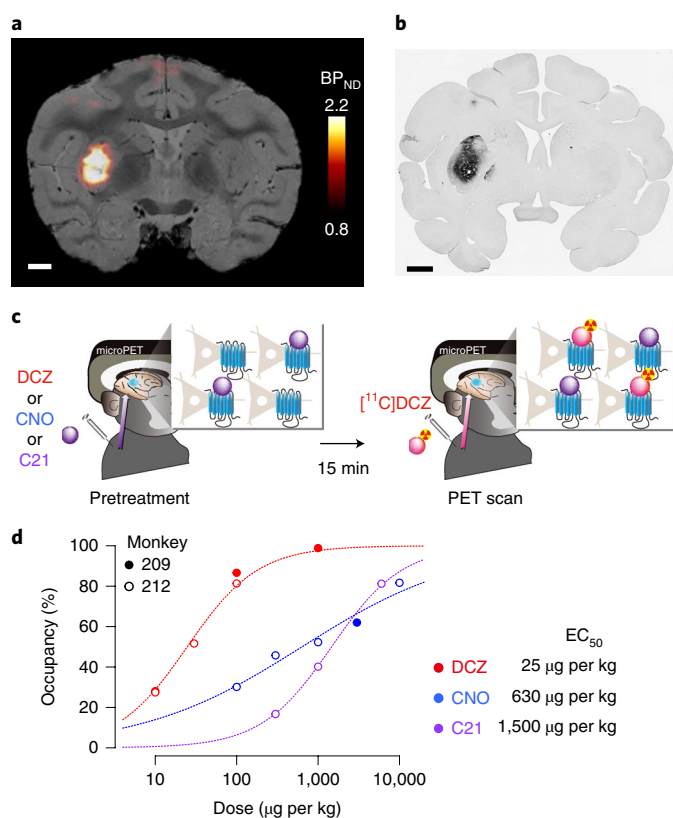
Fig. 2 | [11C]DCZ PET visualizes DREADD expression and measures the agonist dose–occupancy relationship. a, A coronal section of a parametric [11C]DCZ PET image of specific binding (BP_{ND}) overlaying an MR image of monkey 209 expressing hM4Di in the putamen. **b**, An anti-hM4 staining section corresponding to the image in **a**. Scale bars, 5 mm (**a** and **b**). **c**, Illustration of the occupancy study. Monkeys underwent a [11C]DCZ PET scan 15 min after i.v. injection of non-radiolabeled DCZ, CNO or C21. **d**, Occupancy of hM4Di plotted as a function of DCZ, CNO or C21 dose. Filled and open circles represent data obtained from monkeys 209 and 212, respectively. Dotted curves are the best-fit Hill equation for the data. ED_{50} indicates the agonist dose inducing 50% occupancy. Hill coefficient (*n*) and coefficient of determination (R^2) values are as follows: DCZ: $n = 1$, $R^2 = 0.99$; CNO: $n = 0.44$, $R^2 = 0.96$; C21: $n = 1$, $R^2 > 0.99$.

DREADD manipulation. We previously used PET imaging to measure the relationship between CNO dose and the degree of hM4Di receptor occupancy, and provided a reasonable upper CNO dose (≤10 mg per kg); these doses successfully induced behavioral alterations in monkeys, while higher doses did not increase occupancy[6]. To quantify the relationship between DCZ dose and hM4Di occupancy, we performed [11C]DCZ PET scans 15 min after i.v. bolus injection of non-radiolabeled DCZ (10, 30, 100 and 1,000 μg per kg) in two monkeys (Fig. 2c). With increasing doses of non-radiolabeled DCZ, specific binding of [11C]DCZ decreased at the hM4Di vector injection site, while the decrease at the contralateral control site was limited. We determined the occupancy as a reduction of BP_{ND} at the target region over the control side relative to baseline. The relationship between the occupancy of hM4Di and DCZ dose was fit to a Hill equation with a coefficient (*n*) equal to approximately 1 (Fig. 2d; Methods), which indicates that DCZ binds non-cooperatively. The data also suggest that a reasonable dose range of DCZ for monkey studies is ≤100 μg per kg: occupancy increases linearly based on the logarithmic dose in this range, while higher doses would contribute to a minimal increase in occupancy as predicted based on standard receptor–ligand relationships.

Additional occupancy studies with CNO and C21 revealed that higher doses were required to occupy hM4Di (Fig. 2d). The dose–occupancy relationship of C21 indicated its binding property (Hill coefficient, $n = 1$) was similar to DCZ, while that of CNO ($n = 0.44$) might reflect complex kinetics of CNO metabolism and excretion. We estimated that the dose required for 50% occupancy (ED_{50}) for DCZ and compared it with those for CNO and C21. The ED_{50} for DCZ was 25 μg per kg, which is 24-fold and 60-fold smaller than for CNO (630 μg per kg) and C21 (1,500 μg per kg), respectively (Fig. 2d).

Pharmacokinetic (PK) studies demonstrated that DCZ administration (100 μg per kg, i.v.) yielded a maximum concentration of DCZ in the cerebrospinal fluid (CSF; ~10 nM) at 30 min post-injection, which was maintained for at least 2 h in monkeys (Fig. 3a, right). A similar level of DCZ in CSF (~10 nM) was observed at 60 min and later following intramuscular (i.m.) administration (Fig. 3b, right). The DCZ concentration was higher than its K_i value for hM4Di in antagonist radioligand binding studies (4.2 nM; Table 1) and far below its K_i value for numerous endogenous channels, receptors and transporters (>50 nM; Fig. 1b). We did not detect any major metabolites of DCZ in the CSF (Fig. 3a,b, right) in monkeys. Collectively, these results suggest that a low systemic dose of DCZ (that is, 100 μg per kg) affords a sufficient concentration of DCZ for hM4Di DREADD binding in vivo for at least 2 h without the detection of metabolites (Fig. 3d) in monkeys.

We also found that DCZ was rapidly available in the mouse brain following intraperitoneal (i.p.) administration (Fig. 3c). The DCZ concentration was ~6-7 nM in CSF and ~100 nM in brain tissue 30 min after administration (Fig. 3c). As the free (unbound) fraction of drug is key for determining the amount of drug that can bind a target protein, we quantified brain protein binding. Such analysis revealed that the fraction of DCZ unbound to mouse brain tissue was about 7.5% (at 1 μM test concentration), which indicates that a major fraction of DCZ binds nonspecifically to brain proteins, as previously described for many CNS-active compounds[17,18]. The free DCZ concentration in CSF was comparable in mice (6–7 nM) and monkeys (~10 nM). Unlike the PK profiles in monkeys, DCZ concentrations in mice rapidly declined and were undetectable at 2 h in both brain tissue and CSF. It is unsurprising that the PK properties of DCZ differ in mice and monkeys, as species differences in the PK properties of CNS-active drugs are well documented[19]. Although C21, the desmethyl metabolite of DCZ (Fig. 3d), was abundant in plasma, C21 was negligible in CSF (<0.2 nM, ~3% of DCZ at 30 min) (Fig. 3c).

DCZ is a potent in vitro DREADD agonist. We next quantified the in vitro agonist activity of DCZ for muscarinic-based DREADDs and compared its potency with several previously reported agonists. We first performed in vitro bioluminescence resonance energy transfer (BRET) assays, which directly measure agonist-induced G protein dissociation, the most proximal signaling event downstream of GPCR activation, with minimal potentiation due to so-called 'receptor reserve' or downstream signal amplification[20]. Using BRET-based assays, DCZ was a potent hM3Dq agonist ($EC_{50} = 0.13$ nM; 95% confidence interval (CI) = 0.09–0.21)—comparable to clozapine (hM3Dq$EC_{50} = 0.09$ (CI = 0.06–0.15) nM)—and about 40-fold and 100-fold more potent than C21 (hM3Dq$EC_{50} = 5.2$ (CI = 3.7–7.3) nM) and CNO (hM3Dq$EC_{50} = 15$ (CI = 8.8–25) nM), respectively (Fig. 4a). DCZ was also a potent agonist for hM4Di (hM4Di$EC_{50} = 0.081$ (CI = 0.042–0.16) nM), which is again comparable to clozapine (hM4Di$EC_{50} = 0.051$ (CI = 0.027–0.097) nM), but with about 30-fold and 90-fold greater potency than C21 (hM4Di$EC_{50} = 2.6$ (CI = 1.6–4.4) nM) and CNO (hM4Di$EC_{50} = 7.3$ (CI = 3.6–15) nM) (Fig. 4b), respectively.

Superior in vitro potency of DCZ over C21 and CNO was also demonstrated in a calcium mobilization assay for hM3Dq[12] and for inhibition of cyclic AMP accumulation for hM4Di; importantly,
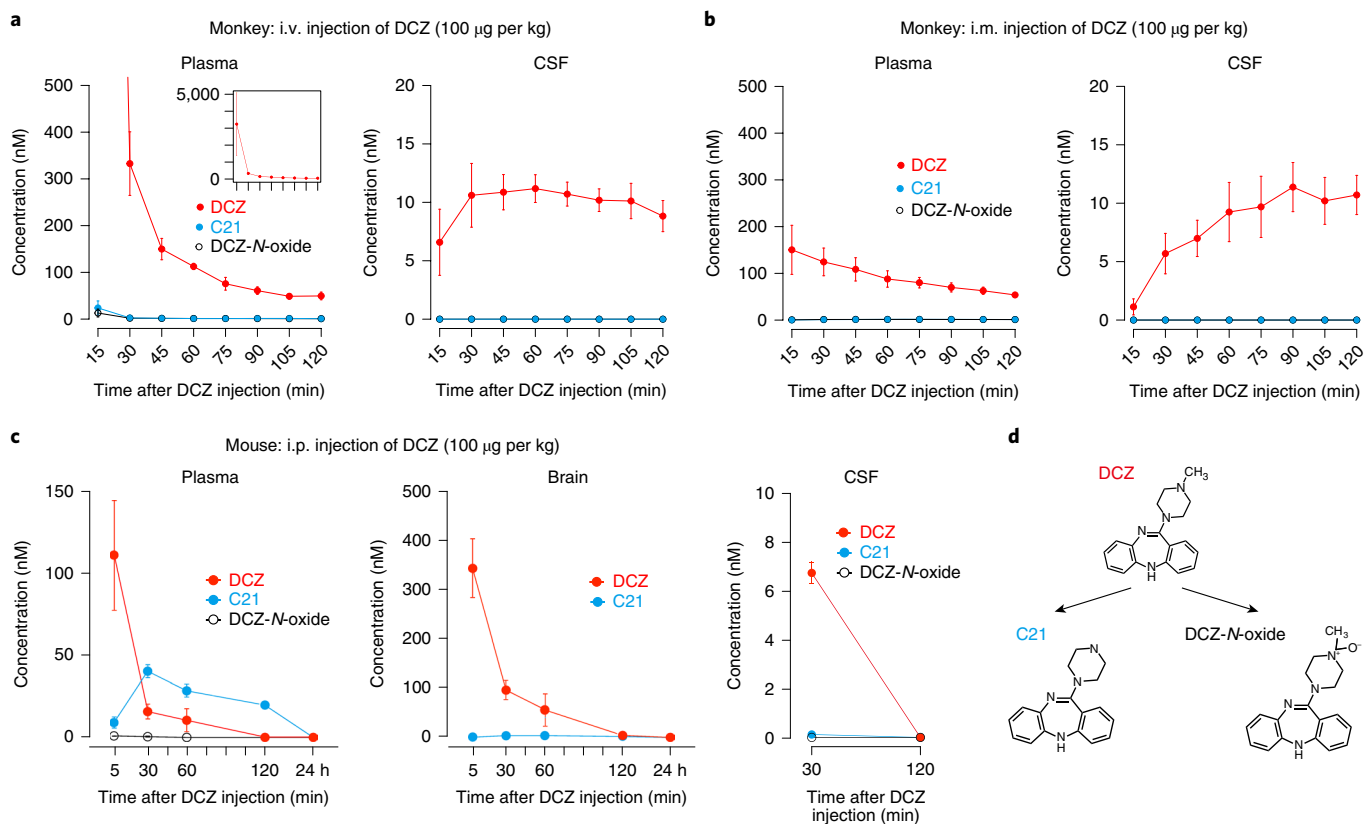
Fig. 3 | Time–concentration profiles of DCZ and its metabolites in monkeys and mice. a, Plasma and CSF concentrations of DCZ and its major metabolites (C21 and DCZ-*N*-oxide) following i.v. injection (100 μg per kg). Data were collected from four monkeys and are shown as the mean ± s.e.m. The inset shows the full-scale plot. **b**, Same as **a**, but following i.m. injection. **c**, Plasma, brain and CSF concentrations of DCZ, C21 and DCZ-*N*-oxide following i.p. injection of DCZ (100 μg per kg). Data were collected from three or four mice and are shown as the mean ± s.e.m. **d**, Major routes of DCZ metabolism leading to C21 and DCZ-*N*-oxide and their structures.

no effect of DCZ was observed in the absence of DREADD expression (Supplementary Fig. 3a–c). To further evaluate potential DCZ off-target agonist actions, we assessed its agonist activity at 318 endogenous GPCRs using an arrestin recruitment assay platform[21]. While DCZ was a potent agonist for hM3Dq and hM4Di, it did not display noticeable agonistic activity for any of the 318 tested wild-type GPCRs at <10 nM, the typical concentration that could be reached with the dose used (Supplementary Fig. 3d–l). Taken together, these results imply that the agonism of DCZ is apparently selective for hM3Dq and hM4Di.

DCZ selectively and rapidly enhances neuronal activity via the hM3Dq DREADD in vivo. We next examined the agonist actions of DCZ on DREADDs and its time course in vivo using two-photon calcium imaging in mice expressing hM3Dq. AAV vectors carrying the GCaMP6s genes (AAV-DJ-rSyn-GCaMP6s) and hM3Dq construct (AAV2-CMV-hM3Dq) were co-injected into the barrel cortex (Fig. 4c). At 28 days post-injection, in vivo hM3Dq expression was visualized by [¹¹C]DCZ PET as a high radioligand binding region at the injection site (Fig. 4d; Supplementary Fig. 1b, right). Given its high potency in vitro, we used DCZ at a dose of 1 μg per kg. Shortly after i.p. injections of DCZ, transient and repetitive increases in fluorescence signals were observed in the soma of hM3Dq-expressing neurons (Fig. 4e,f). On average, relative fluorescence signal changes from baseline (Δ*F*/*F*) rapidly increased (τ = 3 min) and became significant at 5 min post-injection (*P* < 0.01, one-way analysis of variance (ANOVA) with post hoc Dunnett test). Δ*F*/*F* values achieved their peak at about 10 min, plateaued for at least 150 min, and then returned to the baseline levels at 4 h

post-injection (Fig. 4g, red; *P* = 0.53). Vehicle injection did not change the activity of the same neuronal population (Fig. 4g, cyan). The DCZ-induced increases in fluorescence signals were apparently mediated by hM3Dq because DCZ did not alter the signal in mice without DREADD expression (Fig. 4g, black). Although DCZ induced strong activity changes, it did not cause long-term apparent desensitization to hM3Dq-positive neurons after recovery, since the neurons demonstrated a reproduced chemogenetic activation by the second DCZ dose and a replicated response to whisker stimulation (Supplementary Fig. 4).

To compare the in vivo agonist efficacy of DCZ with those of other ligands, we used 100-fold higher doses (100 μg per kg, i.p.) of CNO and C21 because they require higher doses to occupy and activate DREADDs (Figs. 2d and 4a). Although administration of CNO and C21 increased Δ*F*/*F* of hM3Dq-expressing neurons, their peak values were less than 40% of that of DCZ (Fig. 4g, blue and purple). Moreover, the kinetics of CNO were relatively slow (τ = 17 min), with the upward trend lasting for 30 min post-injection and then plateauing (Fig. 4g, blue), as observed in a previous electrophysiological study[22]. While C21 quickly increased Δ*F*/*F* (τ = 4 min), the increase became significant only at 30 min post-injection or later (Fig. 4g, purple). Thus, DCZ rapidly and reversibly activates hM3Dq-expressing neuronal populations in mice in vivo, with higher efficacy and potency than C21 or CNO.

Rapid and reversible chemogenetic neuronal control was also observed in monkeys after systemic DCZ administration. A total of four monkeys were injected with AAV2-CMV-hM3Dq into the unilateral amygdala (Fig. 5a; one used for electrophysiology and the other three for activation imaging; see below). At 48–66 days
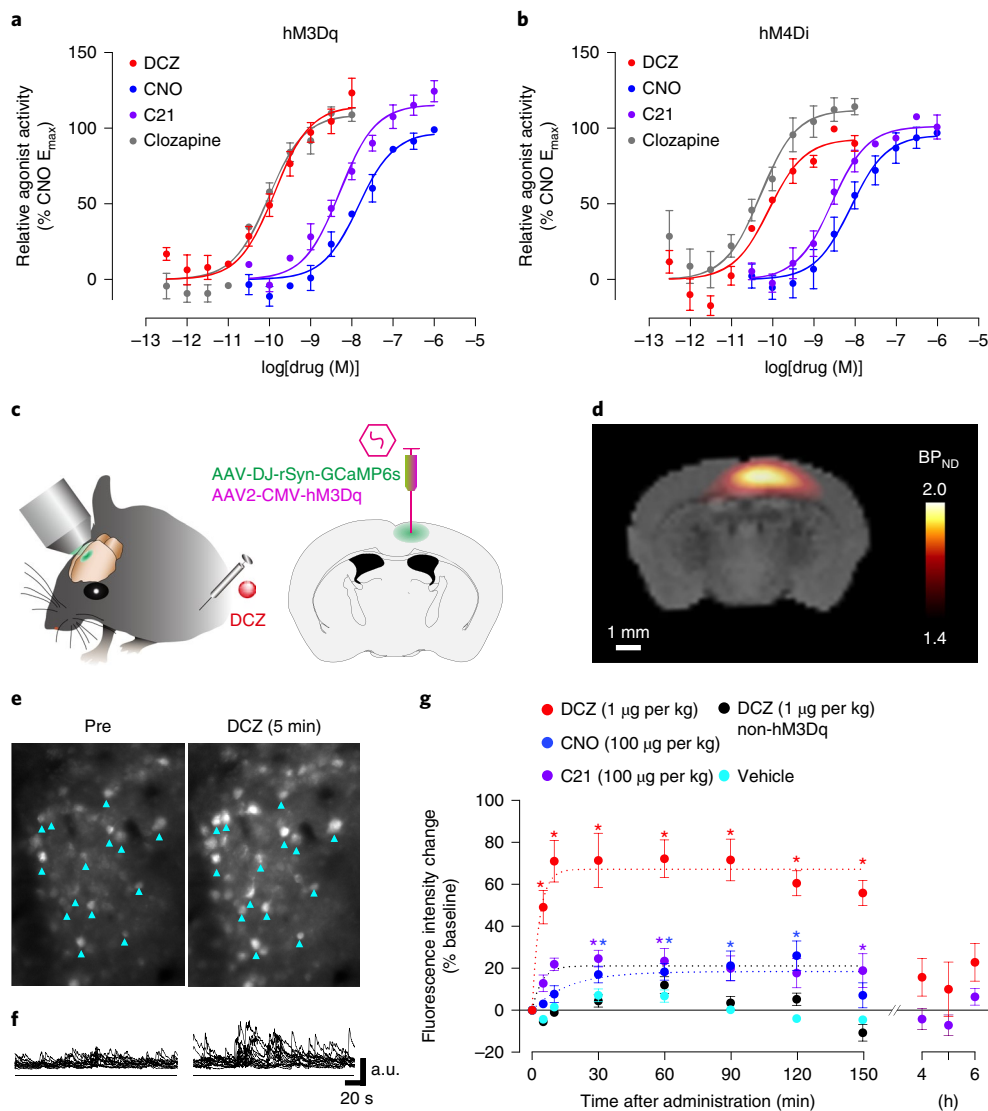
Fig. 4 | In vitro potency and in vivo efficacy of DCZ for DREADDs. a,b, BRET-based estimation of agonist potency and efficacy at hM3Dq and hM4Di in HEK293T cells. Shown are the mean ± s.e.m. of $N = 3$ independent biological replicates (each of which had duplicate technical replicates) of dose–response curves for hM3Dq using a G_q-based BRET sensor and hM4Di using a G_{ii}-based BRET sensor. **c**, Illustration of two-photon calcium imaging and location for co-injection of AAV2-CMV-hM3Dq and AAV-DJ-rSyn-GCaMP6s. **d**, A parametric image of specific binding of [^{11}C]DCZ overlaying an MR image. **e**, Time-averaged two-photon images of GCaMP6 of pre-injection (left) and 5 min post-DCZ injection (1 µg per kg, i.p.) (right). Arrowheads indicate the neurons measured. **f**, Raw fluorescence signals in 14 representative neurons from imaging in **e** (a.u., arbitrary units). **g**, Fluorescence intensity change (mean ± s.e.m. from baseline) as a function of post-injection time. Data were obtained from neurons ($N = 58$) in 4 hM3Dq-expressing mice and neurons ($N = 30$) in 2 non-hM3Dq mice. Curves represent exponential fits to the data. Asterisks represent significant difference ($P < 0.01$, one-way ANOVA with post hoc Dunnett test) from pre-injection.

post-injection, in vivo hM3Dq expression was visualized by [^{11}C] DCZ PET as a high radioligand binding region at the injection site (Fig. 5b), which was confirmed by immunohistochemistry (Supplementary Fig. 5). We recorded local field potentials (LFPs) from the hM3Dq-positive area of one monkey using a multisite linear probe, the location of which was confirmed by computer tomography (CT)–PET fusion images (Fig. 5b). To the best of our knowledge, there have been no prior reports of a monkey chemogenetic study using hM3Dq. Therefore, we applied the same dose of DCZ (1 µg per kg) as in mice to avoid potential risks of excitotoxicity or seizure due to excessive neuronal activation. In the amygdala, LFP gamma band activity, which correlates with firing of local populations of neurons[23], increased significantly from baseline by administration of DCZ ($t(26) = 7.3$, $P = 8.7 \times 10^{-8}$, paired t-test), but not by vehicle ($t(25) = 0.28$, $P = 0.78$; Fig. 5c,d). As control, when

we placed an electrode outside the hM3Dq-positive sites, significant changes in gamma power were not observed after DCZ administration ($t(10) = 0.46$, $P = 0.65$; Fig. 5d). LFP gamma power rapidly increased ($\tau = 4$ min) from baseline and became significant at 5 min after DCZ administration, and this significant increase lasted for at least 45 min ($P < 0.01$, one-way ANOVA with post hoc Dunnett test; Fig. 5e).

DCZ selectively induces hM3Dq-mediated metabolic activity. We next performed a PET study with [^{18}F]fluorodeoxyglucose (FDG) to examine whether DCZ induces dose-dependent and DREADD-selective changes in regional brain glucose metabolism, an index of brain neuronal/synaptic activation[24–26]. Three monkeys expressing hM3Dq in the unilateral amygdala underwent [^{18}F] FDG PET imaging following systemic DCZ or vehicle injection
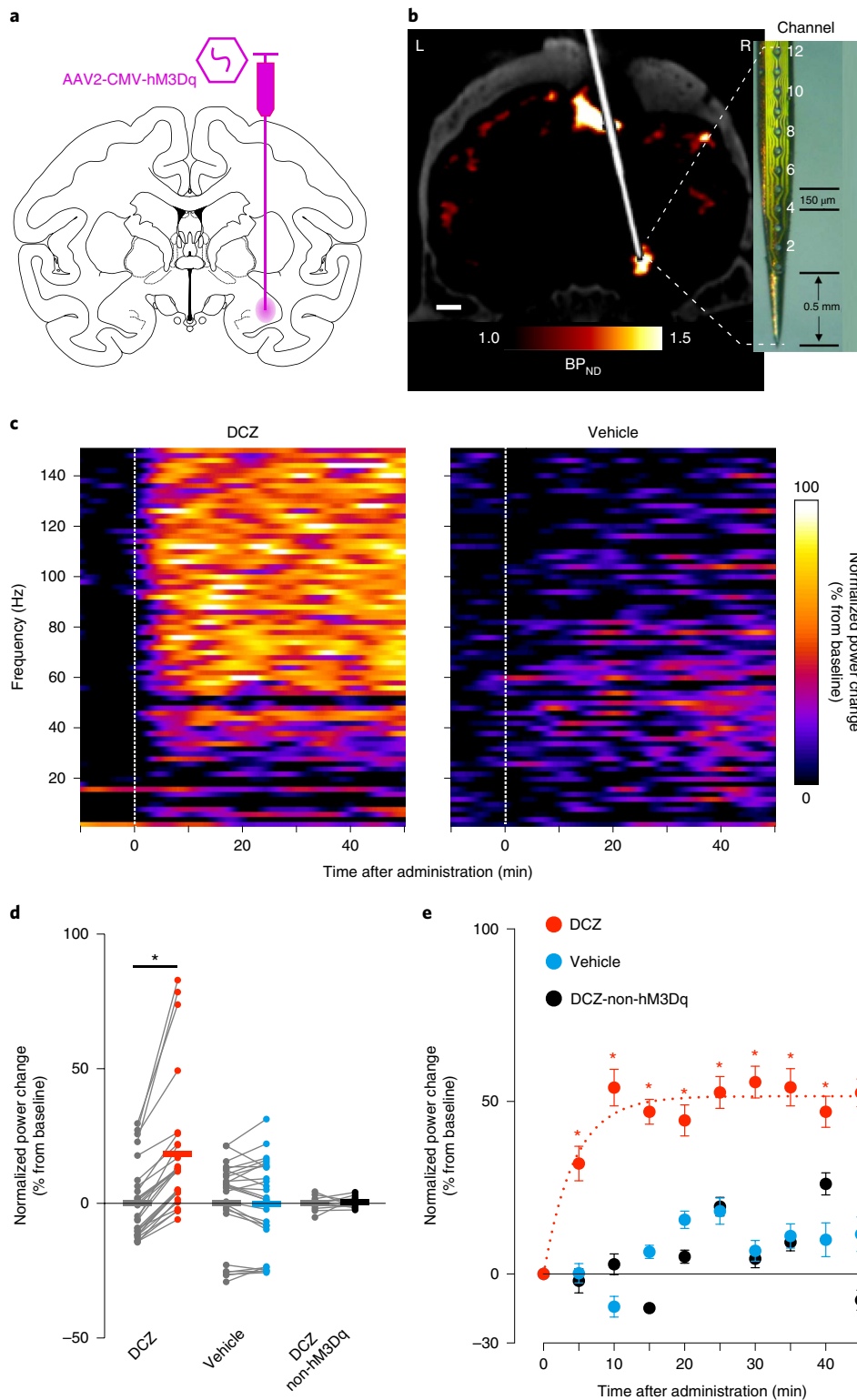
Fig. 5 | DCZ rapidly drives activation of hM3Dq-expressing neuronal population in monkey. a, Illustration of viral vector (AAV2-CMV-hM3Dq) injection into one side of the amygdala. **b**, A coronal PET image overlaying a CT image, demonstrating that recording contacts on a multichannel electrode (shown on right) were located in an hM3Dq-expressing region, which was visualized as a high [^{11}C]DCZ binding site. The high binding observed in the dorsomedial surface corresponds to a site of biological reaction within the recording chamber. Scale bar, 5 mm. **c**, Representative LFP activity changes after DCZ (left) and vehicle administration (right). **d**, Normalized gamma (40 Hz) power change (mean ± s.e.m. from baseline) 10–20 min after i.v. administration of reagents. Data were obtained from an hM3Dq-positive region (DCZ and vehicle; $N = 27$ and 26 channels, respectively, acquired across 4 sessions) and non-hM3Dq expressing sites (DCZ-non-hM3Dq; $N = 11$ channels, acquired within 1 session). Gray bars indicate baseline. Asterisk represents significant difference from baseline. DCZ $t(26) = 7.3$, $P = 8.7 \times 10^{-8}$; vehicle $t(25) = 0.28$, $P = 0.78$; DCZ-non-hM3Dq $t(10) = 0.46$, $P = 0.65$. **e**, Plots of the normalized power change (mean ± s.e.m. from baseline) as a function of time after vehicle or DCZ administration. The curve represents an exponential fit to the data. Asterisks represent a significant difference ($P < 0.01$, one-way ANOVA with post hoc Dunnett test) from baseline. Data were obtained from one animal.
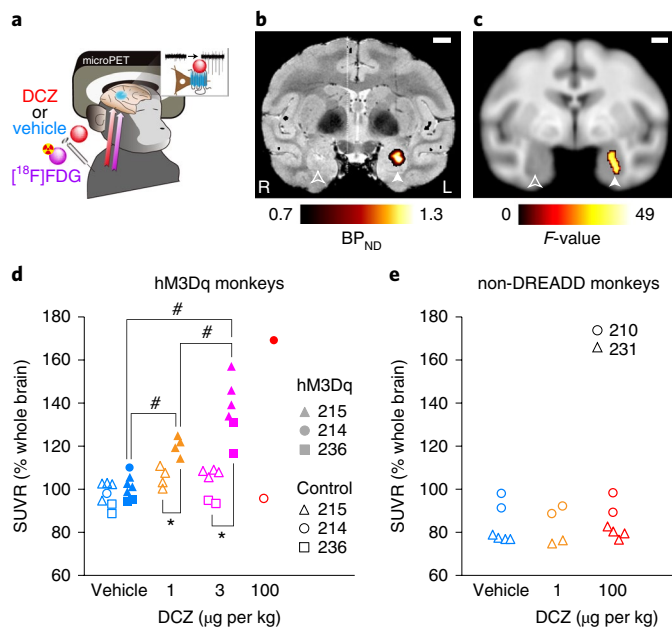
Fig. 6 | DCZ selectively induces metabolic changes in an hM3Dq-expressing region in a dose-dependent manner. a, Illustration of DREADD activation imaging with [18F]FDG. Following the administration of DCZ at effective doses, [18F]FDG was injected and a PET scan was performed to assess DREADD-induced brain metabolic changes. **b**, A coronal PET image overlaying an MR image representing specific [11C] DCZ binding (BP_{ND}) in monkey 215. Filled and open arrowheads indicate the hM3Dq-expressing and control region in the amygdala, respectively. Scale bar, 5 mm. **c**, Brain areas with significantly increased [18F]FDG uptake after DCZ injection (3 μg per kg, $N = 6$ scans) compared to vehicle ($N = 6$) overlaid on an MR image template (uncorrected $P < 0.001$, $F_{(1,8)} > 20.25$, one-way ANOVA within subject, monkeys 215 and 236). The significance level is given as an F-value represented on a color scale. **d**, The relationship between the dose of DCZ administration and standardized FDG uptake (SUVR) in monkeys expressing hM3Dq in the amygdala. Filled and open symbols are the values at hM3Dq-expressing amygdala and contralateral control region, respectively. *$P < 0.01$, paired t-test (for 1 μg per kg DCZ: $t(3) = 6.0$, $P = 0.009$; for 3 μg per kg DCZ: $t(5) = 9.7$, $P = 2.0 \times 10^{-4}$). #$P < 0.05$, one-way ANOVA with post hoc Tukey test ($F(2,14) = 25.06$, $P = 2.4 \times 10^{-5}$; vehicle versus 1 μg per kg: $P = 0.013$; vehicle versus 3 μg per kg: $P = 1.6 \times 10^{-5}$; 1 μg versus 3 μg per kg: $P = 0.03$). **e**, Same as **d**, but for the amygdala of control monkeys without hM3Dq vector injection (non-DREADD monkeys 210 and 231). There was no significant dose effect (one-way ANOVA, $F(2,12) = 2.29$, $P = 0.14$).

(Fig. 6a–c). We found that FDG uptake at the hM3Dq-positive amygdala significantly increased after injections of 1 and 3 μg per kg DCZ doses (paired t-test, $P < 0.01$ for each dose), and this was reproducible without a reduction due to repetitive activations (Fig. 6d). The increase of FDG uptake occurred in a dose-dependent manner at the hM3Dq-positive amygdala region, while uptake at the contralateral control area was unchanged (one-way ANOVA, main effect of dose, $F(2,14) = 25.06$, $P = 2.4 \times 10^{-5}$; Fig. 6d). Voxel-wise statistical analysis further revealed a significant increase in FDG uptake after DCZ administration (3 μg per kg, i.v.) occurred exclusively at the hM3Dq-positive area ($P < 0.001$, uncorrected; Fig. 6b,c). In control monkeys without hM3Dq vector injection (non-DREADD; $N = 2$), administration of DCZ (1 or 100 μg per kg) did not change FDG uptake in the amygdala (one-way ANOVA, main effect of dose, $F(2,12) = 2.29$, $P = 0.14$; Fig. 6e). Voxel-wise statistical analysis demonstrated that no significant metabolic change was detected throughout the entire brain following a high dose of DCZ injection

(100 μg per kg) in control monkeys, which confirms that the off-target effect of DCZ is undetectable in vivo by this measure. These results suggest that DCZ induces a dose-dependent increase of chemogenetic neuronal excitation as measured by metabolic change with no significantly detectable off-target effects.

DCZ selectively induces behavioral deficits in hM4Di-expressing monkeys. Finally, we sought to modify cognitive behavior using inhibitory DREADDs and DCZ. We targeted the prefrontal cortex (PFC), especially sectors around the principal sulcus corresponding to Brodmann's area 46, which is responsible for spatial working memory and executive function. To implement chemogenetic silencing, two monkeys received multiple injections of an AAV vector carrying genes encoding hM4Di (AAV1-hSyn-hM4Di-IRES-AcGFP) bilaterally into the dorsal and ventral banks of the principal sulcus (Fig. 7a). [11C]DCZ PET confirmed that in vivo hM4Di expression covered the bilateral target regions (Fig. 7b). We used a spatial delayed-response task (Fig. 7c), which is frequently employed as a sensitive probe of spatial working memory[7,27]. Compared to vehicle administration, i.m. administration of DCZ (100 μg per kg) significantly impaired the performance of the delayed-response task (two-way ANOVA with treatment × delay, main effect of treatment, $F(1,24) = 63.53$, $P = 3.4 \times 10^{-8}$, and $F(1,24) = 188.5$, $P = 7.3 \times 10^{-13}$ for monkeys 229 and 245, respectively; Fig. 7d). Impairment was more severe in the trials with longer delays (two-way ANOVA with treatment × delay, interaction, $F(2,24) = 11.25$, $P = 3.6 \times 10^{-4}$, and $F(2,24) = 188.5$, $P = 4.3 \times 10^{-4}$ for monkeys 229 and 245, respectively), which suggests that it was attributable to loss of working-memory function. Impairment of the delayed-response task appeared shortly after administration (<10 min) and lasted for at least 2 h (t-test, $P < 0.05$ for all test time periods; Fig. 7e), but disappeared at 24 h (two-way ANOVA with treatment × delay, main effect of treatment, vehicle versus 24 h after DCZ: $F(1,24) = 0.60$, $P = 0.45$, and $F(1,24) = 0.94$, $P = 0.34$ for monkeys 229 and 245, respectively; DCZ versus 24 h after DCZ: $F(1,24) = 59.48$, $P = 6.0 \times 10^{-8}$, and $F(1,24) = 171.6$, $P = 2.0 \times 10^{-12}$ for monkeys 229 and 245, respectively; Fig. 7d). The behavioral effect with DCZ was reproducible without attenuation due to repetitive DREADD activation (Fig. 7f). Without a screen during the delay period, DCZ did not affect the performance of the monkey, which indicates that the impairment was unlikely attributable to deficits in motor function, visual perception or general motivation (Fig. 7g). We confirmed that DCZ alone did not produce any significant effects on spatial working memory in non-DREADD monkeys ($N = 2$, including monkey 245, one of the two monkeys that was tested before vector injection; Fig. 7h). Additional behavioral examinations in three other non-DREADD monkeys using a reward-size task further corroborated that significant side effects of DCZ injection (100 μg per kg, i.m.) were undetectable on motor or motivational functions (Supplementary Fig. 6). These results demonstrate that DCZ enables a rapidly and reversibly induced behavioral change through activating muscarinic-based DREADDs without discernible side effects.

Discussion

Here, we report that the new DREADD agonist DCZ represents an extremely potent, highly brain penetrant and selective actuator for hM3Dq and hM4Di DREADDs in both mice and monkeys. The properties of DCZ described here demonstrate that it can be adopted as a preferred, fast-acting chemogenetic actuator with minimal off-target actions, thereby enhancing opportunities for investigating the causal link between neuronal activity and behavior with high translational potential.

Several features of DCZ indicate its superiority as a chemogenetic actuator over prior agonists. First, DCZ exhibits DREADD-selective binding both in vitro and in vivo. Radioligand binding assays demonstrated that DCZ is selective for hM3Dq and hM4Di. PET imaging

demonstrated that DCZ has substantially improved selectivity compared to clozapine, whereby DCZ exhibited decreased off-target binding while retaining similar potency at muscarinic DREADDs as clozapine. Second, DCZ has good brain concentration profiles and biostability. PET imaging revealed that systemically administered DCZ occupied hM4Di DREADDs with a similar occupancy to CNO or C21 at ~20-fold or 60-fold lower doses, respectively. PK studies confirmed that DCZ is rapidly accumulated in mouse brains and monkey CSF, while its metabolites are negligible. Third, DCZ has high potency for muscarinic DREADDs. In vitro assays revealed that hM3Dq was activated by substantially lower concentrations of DCZ compared to CNO and C21. DCZ did not display noticeable agonist potencies for any of the 318 off-target GPCRs tested. Indeed, binding assays at a number of GPCRs, channels and transporters screened by the National Institute of Mental Health Psychoactive Drug Screening Program (NIMH PDSP) showed that DCZ had modest affinity (55–87 nM) for a few GPCRs, low affinity (100–1,000 nM) for several GPCRs and minimal activity (>1,000 nM) at most CNS targets tested. In short, DCZ has a higher selectivity for DREADDs than clozapine and is capable of occupying and activating DREADDs at a lower dose than CNO and C21, thus offering a greater effective window than the prior DREADD ligands.

CNO has repeatedly been shown to have relatively slow kinetics for neuronal activation via hM3Dq. Following systemic administration, increases in activity begin at around 5–10 min and reach a maximum at 45 min or later[22]. Because bath application of CNO immediately increases the firing rate of hM3Dq-expressing neurons in slice preparations[22], the relatively slow activation appears to reflect the slow kinetics of CNO uptake in the brain. Moreover, the

major effects on DREADDs may be exerted by its metabolite clozapine rather than CNO itself[8], for which metabolism is non-negligeble in rodents[8,9] and in monkeys with slower delivery (for example, subcutaneous injection[10]). Although the concentration of metabolized clozapine is minimal in monkeys with rapid i.v. delivery of CNO[6,28], the brain uptake of CNO is considerably low (Fig. 1i). In contrast, DCZ quickly penetrates into the brain and induces a rapid onset of excitability of hM3Dq-positive neuronal populations, as demonstrated by two-photon calcium imaging in mice and by electrophysiological recording in monkeys (Figs. 4 and 5). Thus, DCZ combined with muscarinic-based DREADDs provides a superior platform for examining the effects of rapid and sustainable chemogenetic neuronal modulation. For example, single-unit or in vivo patch-clamp recording studies, for which long-term (30–60 min) maintenance is technically demanding, would greatly benefit from the rapid action of the DCZ–DREADD system. Such a rapid chemogenetic

Fig. 7 | DCZ selectively and rapidly induces spatial working-memory deficit in monkeys expressing hM4Di in the PFC. a, Illustration of the location of viral vector injections. AAV1-hSyn-hM4Di-IRES-AcGFP was bilaterally injected into the dorsal and ventral banks of the principal sulcus. **b**, A coronal parametric image of specific binding of [^{11}C]DCZ overlaying an MR image in monkey 229. Open and filled arrowheads represent the dorsal and ventral borders of the target regions, respectively. Scale bar, 5 mm. **c**, Illustration of the spatial delayed-response task. After the monkey was shown the baited well (Cue), the screen was placed for 0.5, 5 or 10 s (Delay). The monkey obtained the food if they reached for the correct food well and removed the cover plate (Response). **d**, Correct performance rates (mean ± s.e.m.) of the spatial delayed-response task with 0.5-, 5- and 10-s delays after vehicle administration ($N = 5$ sessions), DCZ administration (100 μg per kg, i.m.; $N = 5$) and 24 h after DCZ administration ($N = 5$) in two monkeys expressing hM4Di in the PFC. Note that monkey 245 was also examined before vector injection (Supplementary Fig. 6c, right). The behavioral testing began immediately after an i.m. administration of either vehicle (2% DMSO in saline) or DCZ, except for 24 h after DCZ. Each dot represents the data in each daily session. **e**, Time course of DCZ effects. Correct performance rates of 5- and 10-s delays as a function of test time for vehicle and DCZ sessions (mean ± s.e.m.; $N = 5$) in monkey 229. The behavioral testings for 0–55 min and 60–115 min were conducted separately. Asterisks represent significant difference (t-test, $P < 0.05$). **f**, Correct performance rates (mean of 5- and 10-s delays) as a function of session number in monkeys 229 and 245. **g**, Correct performance rates of the non-memory task after vehicle ($N = 5$ sessions) and DCZ administration (100 μg per kg, i.m.; $N = 5$) in monkey 229. There was no main effect of treatment (two-way ANOVA, $F_{(1,16)} = 1.1 \times 10^{-8}$, $P = 1.0$). **h**, There was no significant effect of DCZ for the delayed-response task in two control monkeys (226 and 245) without hM4Di vector injection (two-way ANOVA, main effect of treatment: $F_{(1,16)} = 0.03$, $P = 0.87$ and $F_{(1,16)} = 1.16$, $P = 0.30$ for monkeys 226 and 245, respectively). Correct performance rates with 5- and 10-s delays after vehicle ($N = 5$ sessions) and DCZ administration (100 μg per kg, i.m.; $N = 5$) are shown. Note that the data of monkey 245 were obtained before vector injection.

action would also be valuable for future therapeutic applications, for instance, on-demand seizure attenuation[29].

The current results indicate that DCZ can also be utilized for in vivo neuronal silencing by activating hM4Di, an inhibitory DREADD. Our data suggest that a reasonable upper limit of DCZ dose is 100 µg per kg (Fig. 2d), which allows a sufficient concentration of DCZ to be available for hM4Di DREADD binding in vivo for at least 2 h in monkeys. Indeed, a 100 µg per kg dose of DCZ rapidly (<10 min) and reversibly induced spatial working memory deficits in monkeys expressing hM4Di in the PFC (Fig. 7). Given the high agonist potency of DCZ (Fig. 4b), smaller DCZ doses would induce similar or detectable behavioral deficits. With its high selectivity and potency, DCZ will provide potential orthogonality of the muscarinic DREADDs to other classes of chemogenetic tools[2,30], thus providing opportunity for a multiplexed/bimodal control of physiological systems. Moreover, in combination with low-invasive targeted gene delivery methods such as ultrasonic blood–brain barrier opening[31], DCZ may open the potential for targeted, minimally invasive and side-effect-free brain theranostics.

One of the technical difficulties in chemogenetic manipulations, especially for large animals, is the delivery of transgene specifically into a target neuronal population and the accomplishment of stable transgene expression throughout the experimental period. Previous studies have shown that PET imaging with [11C]clozapine or [11C]CNO can visualize hM4Di expression in living mice and monkeys, thereby providing effective tools for noninvasive monitoring of gene expression[6,15]. However, because these ligands display poor DREADD selectivity or brain permeability, the application of DREADD–PET in monkeys was limited to visualization of hM4Di expression in the striatum. The present study demonstrated that [11C]DCZ is an exceedingly useful PET ligand for visualizing both hM3Dq and hM4Di expression in cortical and subcortical areas of mice and monkeys, with improved specificity compared to [11C]clozapine (Fig. 1). The monitoring of transgene expression is beneficial for long-term behavioral studies and is of great advantage for conducting successful experiments (Fig. 7). In addition to expression monitoring, PET imaging enabled the elucidation of a relationship between a pharmacologically effective dose of DREADD agonists and DREADD occupancy in vivo (Fig. 2d). Moreover, we demonstrated that [11C]DCZ PET enables the visualization of DREADD expression at axon terminal sites (Supplementary Fig. 2). This provides a powerful means for mapping projection areas for pathway-selective activity manipulation[32], which can be induced by local infusion of DREADD agonist; DCZ may be suitable because of its high selectivity and efficacy (Fig. 1).

Although PET imaging data have implied that DCZ has off-target binding in cortical areas, which is possibly due to endogenous receptors with low affinities (Fig. 1g; Supplementary Table 1), the agonist potency of DCZ at DREADDs is in the subnanomolar range and, therefore, when used at a sufficient dose, occupancy on off-targets (~50 nM or higher) can be predicted to be minimal. Indeed, our data further suggest that systemic administration of DCZ at 100 µg per kg or smaller doses would not induce discernible off-target effects on neuronal activity or behavior in monkeys not expressing the muscarinic-based DREADDs (Fig. 6; Supplementary Fig. 6). Since the variability of CSF concentration across subjects and the amount of metabolites for DCZ were much smaller than those for CNO[6] (Fig. 3a), the potential baseline sensitivity to DCZ would be minimal. Therefore, DCZ provides a clear advantage over prior agonists due to its increased reliability (that is, there are minimal concerns about potential off-target effects). However, we cannot completely rule out unanticipated off-target effects because it is impossible to measure the activity of DCZ against every potential endogenous target. Therefore, as with all other neuromodulation technologies, control experiments—here using non-DREADD animals—are recommended. In mice, control experiments are essential

since the current study did not examine an off-target action of DCZ at a high dose; that is, C21, a DCZ metabolite, was detected at very low concentrations in CSF (<0.2 nM; Fig. 3c). Future studies will be required to determine appropriate DCZ doses and the effective time window for mouse chemogenetic experiments.

In conclusion, the characteristics of DCZ described here—its high selectivity, high brain penetrability and biostability—facilitate the rapid and selective modulation of neuronal activity and behavior with muscarinic-based DREADDs in living animals. Given the potential drawbacks of prior DREADD agonists, DCZ will provide clear benefits for many users of muscarinic DREADDs, with increased reliability due to removing concerns about potential off-target responses.

Online content

Any methods, additional references, Nature Research reporting summaries, source data, extended data, supplementary information, acknowledgements, peer review information; details of author contributions and competing interests; and statements of data and code availability are available at https://doi.org/10.1038/s41593-020-0661-3.

References
1. Armbruster, B. N., Li, X., Pausch, M. H., Herlitze, S. & Roth, B. L. Evolving the lock to fit the key to create a family of G protein-coupled receptors potently activated by an inert ligand. *Proc. Natl Acad. Sci. USA* **104**, 5163–5168 (2007).
2. Vardy, E. et al. A new DREADD facilitates the multiplexed chemogenetic interrogation of behavior. *Neuron* **86**, 936–946 (2015).
3. Roth, B. L. DREADDs for neuroscientists. *Neuron* **89**, 683–694 (2016).
4. Grayson, D. S. et al. The rhesus monkey connectome predicts disrupted functional networks resulting from pharmacogenetic inactivation of the amygdala. *Neuron* **91**, 453–466 (2016).
5. Eldridge, M. A. G. et al. Chemogenetic disconnection of monkey orbitofrontal and rhinal cortex reversibly disrupts reward value. *Nat. Neurosci.* **19**, 37–39 (2015).
6. Nagai, Y. et al. PET imaging-guided chemogenetic silencing reveals a critical role of primate rostromedial caudate in reward evaluation. *Nat. Commun.* **7**, 13605 (2016).
7. Upright, N. A. et al. Behavioral effect of chemogenetic inhibition is directly related to receptor transduction levels in rhesus monkeys. *J. Neurosci.* **38**, 1418–1422 (2018).
8. Gomez, J. L. et al. Chemogenetics revealed: DREADD occupancy and activation via converted clozapine. *Science* **357**, 503–507 (2017).
9. Manvich, D. F. et al. The DREADD agonist clozapine N-oxide (CNO) is reverse-metabolized to clozapine and produces clozapine-like interoceptive stimulus effects in rats and mice. *Sci. Rep.* **8**, 3840 (2018).
10. Raper, J. et al. Metabolism and distribution of clozapine-N-oxide: implications for nonhuman primate chemogenetics. *ACS Chem. Neurosci.* **8**, 1570–1576 (2017).
11. Roth, B. L., Sheffler, D. J. & Kroeze, W. K. Magic shotguns versus magic bullets: selectively non-selective drugs for mood disorders and schizophrenia. *Nat. Rev. Drug Discov.* **3**, 353–359 (2004).
12. Chen, X. et al. The first structure–activity relationship studies for designer receptors exclusively activated by designer drugs. *ACS Chem. Neurosci.* **6**, 476–484 (2015).
13. Thompson, K. J. et al. DREADD agonist 21 is an effective agonist for muscarinic-based DREADDs in vitro and in vivo. *ACS Pharmacol. Transl Sci.* **1**, 61–72 (2018).
14. Phillips, S. T. et al. Binding of 5H-dibenzo[b,e][1,4]diazepine and chiral 5H-dibenzo[a,d]cycloheptene analogs of clozapine to dopamine and serotonin receptors. *J. Med. Chem.* **37**, 2686–2696 (1994).
15. Ji, B. et al. Multimodal imaging for DREADD-expressing neurons in living brain and their application to implantation of iPSC-derived neural progenitors. *J. Neurosci.* **36**, 11544–11558 (2016).
16. Farrell, M. S. & Roth, B. L. Pharmacosynthetics: reimagining the pharmacogenetic approach. *Brain Res.* **1511**, 6–20 (2013).
17. Kalvass, J. C., Maurer, T. S. & Pollack, G. M. Use of plasma and brain unbound fractions to assess the extent of brain distribution of 34 drugs: comparison of unbound concentration ratios to in vivo P-glycoprotein efflux ratios. *Drug Metab. Dispos.* **35**, 660–666 (2007).

18. Maurer, T. S., DeBartolo, D. B., Tess, D. A. & Scott, D. O. Relationship between exposure and nonspecific binding of thirty-three central nervous system drugs in mice. *Drug Metab. Dispos.* **33**, 175–181 (2005).

19. Martinez, M. N. Factors influencing the use and interpretation of animal models in the development of parenteral drug delivery systems. *AAPS J.* **13**, 632–649 (2011).

20. Olsen, R.H.J. et al. TRUPATH, an open-source biosensor platform for interrogating the GPCR transducerome. *Nat. Chem. Biol.* https://doi.org/10.1038/s41589-020-0535-8 (2020).

21. Kroeze, W. K. et al. PRESTO-Tango as an open-source resource for interrogation of the druggable human GPCRome. *Nat. Struct. Mol. Biol.* **22**, 362–369 (2015).

22. Alexander, G. M. et al. Remote control of neuronal activity in transgenic mice expressing evolved G protein-coupled receptors. *Neuron* **63**, 27–39 (2009).

23. Buzsáki, G., Anastassiou, C. A. & Koch, C. The origin of extracellular fields and currents—EEG, ECoG, LFP and spikes. *Nat. Rev. Neurosci.* **13**, 407–420 (2012).

24. Michaelides, M. et al. Whole-brain circuit dissection in free-moving animals reveals cell-specific mesocorticolimbic networks. *J. Clin. Invest.* **123**, 5342–5350 (2013).

25. Phelps, M. E. et al. Tomographic measurement of local cerebral glucose metabolic rate in humans with (F-18)2-fluoro-2-deoxy-D-glucose: validation of method. *Ann. Neurol.* **6**, 371–388 (1979).

26. Poremba, A. et al. Species-specific calls evoke asymmetric activity in the monkey's temporal poles. *Nature* **427**, 448–451 (2004).

27. Tsutsui, K.-I., Oyama, K., Nakamura, S. & Iijima, T. Comparative overview of visuospatial working memory in monkeys and rats. *Front. Syst. Neurosci.* **10**, 99 (2016).

28. Allen, D. C. et al. A comparative study of the pharmacokinetics of clozapine *N*-oxide and clozapine *N*-oxide hydrochloride salt in rhesus macaques. *J. Pharmacol. Exp. Ther.* **368**, 199–207 (2018).

29. Kätzel, D., Nicholson, E., Schorge, S., Walker, M. C. & Kullmann, D. M. Chemical–genetic attenuation of focal neocortical seizures. *Nat. Commun.* **5**, 3847 (2014).

30. Magnus, C. J. et al. Ultrapotent chemogenetics for research and potential clinical applications. *Science* **364**, eaav5282 (2019).

31. Szablowski, J. O., Lee-Gosselin, A., Lue, B., Malounda, D. & Shapiro, M. G. Acoustically targeted chemogenetics for the non-invasive control of neural circuits. *Nat. Biomed. Eng.* **2**, 475–484 (2018).

32. Stachniak, T. J., Ghosh, A. & Sternson, S. M. Chemogenetic synaptic silencing of neural circuits localizes a hypothalamus→midbrain pathway for feeding behavior. *Neuron* **82**, 797–808 (2014).

Methods

Subjects. All experimental procedures involving animals were carried out in accordance with the Guide for the Care and Use of Laboratory Animals (National Research Council of the US National Academy of Sciences) and were approved by the Animal Ethics Committee of the National Institutes for Quantum and Radiological Science and Technology.

A total of 16 macaque monkeys (7 rhesus (*Macaca mulatta*) and 9 Japanese monkeys (*Macaca fuscata*); 11 males, 5 females; 2.8–8.0 kg; age 4–10 years) were used (a summary of the subjects used in the experiments is provided in Supplementary Table 2). The monkeys were kept in individual primate cages in an air-conditioned room. A standard diet, supplementary fruits/vegetables and a tablet of vitamin C (200 mg) were provided daily.

Adult hM4Di transgenic mice with C57BL/6j background[15] (male, age >12 weeks) and age-matched non-transgenic littermates or wild-type C57BL/6j mice (male, age >12 weeks; Japan SLC) were used. All mice were maintained in a 12-h light–dark cycle with ad libitum access to standard diet and water.

Viral vector production. AAV2 (AAV2-CMV-hM4Di, AAV2-CMV-KORD, AAV2-CMV-hM3Dq, AAV2-CMV-AcGFP; Figs. 1d, 4c and 5a) and AAV1 (AAV1-hSyn-hM4Di-IRES-AcGFP; Fig. 7a) vectors were produced using a helper-free triple transfection procedure and were purified by affinity chromatography (GE Healthcare). Viral titers were determined by quantitative PCR using Taq-Man technology (Life Technologies). The transfer plasmid was constructed by inserting a complementary DNA fragment and the WPRE sequence into an AAV backbone plasmid (pAAV-CMV, Stratagene). For production of an AAV-DJ vector (AAV-DJ-rSyn-GCaMP6s), a transfer plasmid containing the rat *Synapsin* promoter and cDNA encoding GCaMP6s (Addgene plasmid number 40753) was assembled and transfected with helper-free DJ plasmids (Cell Biolabs). Viral particles were purified using a HiTrap heparin column (GE Healthcare). Viral titers were determined using an AAVpro Titration kit ver2 (Takara).

Surgical procedures and viral vector injections. In monkeys, surgeries were performed under aseptic conditions in a fully equipped operating suite. We monitored body temperature, heart rate, SpO_2 and tidal CO_2 throughout all surgical procedures. Monkeys were immobilized by i.m. injection of ketamine (5–10 mg per kg) and xylazine (0.2–0.5 mg per kg) and intubated with an endotracheal tube. Anesthesia was maintained with isoflurane (1–3%, to effect). Before surgery in monkeys, magnetic resonance (MR) imaging (7 tesla 400 mm/SS system, NIRS/KOBELCO/Brucker) and X-ray CT scans (Accuitomo170, J. Morita) were performed under anesthesia (continuous infusion of propofol 0.2–0.6 mg per kg per min, i.v.). Overlay MR and CT images were created using PMOD image analysis software (PMOD Technologies) to estimate stereotaxic coordinates of target brain structures.

For subcortical injections, monkeys underwent a surgical procedure to open burr holes (~8 mm in diameter) for the injection needle. Viruses were pressure-injected using a 10-μl Hamilton syringe (model 1701 RN, Hamilton) with a 30-gauge injection needle and a fused silica capillary (450-μm outside diameter) to create a 'step' about 500-μm away from the needle tip to minimize backflow. The Hamilton syringe was mounted into a motorized microinjector (Legato130, KD Scientific or UMP3T-2, WPI) that was held by a manipulator (model 1460, David Kopf) on the stereotaxic frame. After the dura mater was opened about 3 mm, the injection needle was inserted into the brain and slowly moved down 2 mm beyond the target and then kept stationary for 5 min, after which it was pulled up to the target location. The injection speed was set at 0.25–0.5 μl min⁻¹. After each injection, the needle remained in situ for 15 min to minimize backflow along the needle. Monkeys 209 and 212 had co-injections of AAV vectors (total 6 μl; 3 μl × 2 different depths in a track) carrying the hM4Di construct (AAV2-CMV-hM4Di; 1.8×10^{13} (monkey 209) and 2.6×10^{13} (monkey 212) particles per ml) and AcGFP genes (AAV2-CMV-AcGFP; 0.7×10^{13} particles per ml) in one side of the putamen and co-injections of AAV vectors (total 6 μl; 3 μl × 2 different depths in a track) carrying κ-opioid-based DREADD construct (AAV2-CMV-KORD; 1.8×10^{13} particles per ml) and AcGFP (AAV2-CMV-AcGFP; 0.7×10^{13} particles per ml) in the other side. Monkeys 214, 215, 233 and 236 had co-injections of AAV vectors (total 6 μl; 3 μl × 2 tracks, 2-mm apart rostrocaudally) carrying the hM3Dq construct (AAV2-CMV-hM3Dq; 1.2×10^{13} particles per ml) and AcGFP genes (AAV2-CMV-AcGFP; 0.7×10^{13} particles per ml) into the left (monkeys 214 and 215) or right (monkeys 233 and 236) amygdala.

Monkeys 229 and 245 had AAV1-hSyn-hM4Di-IRES-AcGFP (3.8×10^{13} particles per ml) injected into the bilateral PFC (Brodmann's area 46). After retracting the skin and galea, the frontal cortex was exposed by removing a bone flap and reflecting the dura mater. Handheld injections were made under visual guidance through an operating microscope (Leica M220, Leica Microsystems), with care taken to place the beveled tip of the Hamilton syringe containing the viral vector at an oblique angle to the brain surface. One person inserted the needle into the intended area of injection and another person pressed the plunger to expel approximately 1 μl. Nine tracks were injected in each hemisphere; one was located 1-mm posterior to the caudal tip of the principal sulcus, and the others were located along the dorsal (4 tracks) and ventral (4 tracks) bank of the principal sulcus posterior to the rostral tip of the ascending limb of the arcuate sulcus

(Fig. 7a). Viral vectors were injected at 3–5 μl per track depending on the depth. Total amounts of viral aliquots injected into the right and left hemispheres were 35 and 37 μl, respectively, for monkey 229, and 44 and 40 μl, respectively, for monkey 245.

In mice, the animals were anesthetized with a mixture of air, oxygen and isoflurane (3–5% for induction and 2% for surgery) via a facemask, and a cranial window (3–4 mm in diameter) was placed over the left somatosensory cortex, centered at 1.8-mm caudal and 2.5-mm lateral from the bregma, according to the Seylaz–Tomita method[33]. On the day of cranial window surgery, AAV vectors carrying genes encoding GCaMP6 (AAV-DJ-rSyn-GCaMP6; 3.5×10^{11} particles per ml) and the hM3Dq construct (AAV2-CMV-hM3Dq; 1.5×10^{13} particles per ml) were co-injected into the barrel cortex using glass needles. A custom metal plate was affixed to the skull with a 7-mm-diameter hole centered over the cranial window. The method for preparing the chronic cranial window has previously been reported in detail[34].

Radioligand competition binding assays. Radioligand binding assays with membrane preparations to determine binding affinity were carried out by the NIMH PDSP (https://pdsp.unc.edu/). Detailed assay protocols are available at the NIMH PDSP website (https://pdsp.unc.edu/pdspweb/?site=assays). NIMH PDSP is directed by B.L.R., University of North Carolina at Chapel Hill, North Carolina, and Program Officer J. Driscoll at NIMH, Bethesda, USA.

BRET experiments. HEK293T cells split into 10-cm plates and maintained in DMEM medium supplemented with 10% fetal bovine serum (FBS) and 1% penicillin–streptomycin (pen–strep) were co-transfected with 1 μg each of hM3D or hM4D and $G\alpha_q$-RLuc8 or $G\alpha i1$-RLuc8, respectively, and 1 μg each of $G\beta_1$ and $G\gamma_2$–GFP2 using TransIT-2020 (Mirus) as the transfection reagent. For negative controls, 1 μg of pcDNA was transfected in place of hM3D or hM4D. After at least 12 h, cells were plated in poly-D-lysine-coated white 96-well microplates (Greiner) in 100 μl of DMEM supplemented with 1% dialyzed FBS and 1% pen–strep at a density of 50,000 cells per well. After at least an additional 12 h, media were aspirated and replaced with 60 μl of assay buffer (1× Hanks' balance salt solution (HBSS), 20 mM HEPES buffer, pH 7.40). Next, 10 μl of 50 μM coelenterazine 400a (NanoLight Technology) was added. After a 5-min incubation, 30 μl of 3× drug (in assay buffer containing 0.3 mg ml⁻¹ ascorbic acid and 0.3% BSA) was added. After an additional 5-min incubation, plates were read for luminescence with a Mithras LB 940 multimodal microplate reader (Berthold Technologies). Data were analyzed by GraphPad Prism 7.0 using the built-in dose–response function and were normalized to the responses produced by CNO. In the presence of RLuc8 substrate coelenterazine, proximal and properly oriented alpha-RLuc8 and gamma–GFP2 produce BRET that reflects the equilibrium association of the heterotrimeric G protein under a given set of conditions. Dissociation of the heterotrimer consequent to receptor activation decreases BRET, and the extent of this decrease is dose-dependent. Since this assay directly measures G-protein dissociation, which is the most proximal signaling event downstream of GPCR activation, measurements made by this assay are relatively insensitive to receptor reserve and signal amplification (see Olsen et al.[20] for details regarding BRET assays and construct design).

In vitro cAMP assays. G_i-mediated inhibition of cAMP production assays were performed in transiently transfected HEK293T cells. Briefly, HEK293T cells, transfected overnight with GloSensor plasmid (Promega) and receptor DNAs, were plated (10–15,000 cells per 40 μl per well) in poly-L-lysine-coated white 384-well clear-bottom cell culture plates in DMEM with 1% dialyzed FBS. After 16–20 h, cells were removed from medium and stimulated with ligands prepared in HBSS, 20 mM HEPES, 0.1% BSA, pH 7.4, for 15 min, followed by 0.1 μM isoproterenol (final concentration) in GloSensor reagent. Luminescence was read on a Wallac TriLux Microbeta counter (PerkinElmer). Results were normalized to the CNO activity and analyzed using the built-in dose–response function in GraphPad Prism 7.0.

In vitro calcium mobilization (FLIPR) assays. HEK293T cells stably expressing hM3Dq or hM3 receptors were used for G_q-mediated calcium mobilization assays. Assays were performed according to published procedures[12]. More detailed assay protocols are available at the NIMH PDSP website (https://pdsp.unc.edu/pdspweb/?site=assays).

GPCRome screening (PRESTO-Tango) assays. Potential agonist activity at the human GPCRome was measured using the PRESTO-Tango assay as previously described[21].

Brain protein-binding assays. The unbound fraction of DCZ in brain tissue was measured using an equilibrium dialysis method. PBS solutions containing mouse brain homogenates (20%) and DCZ (final concentrations of 10, 100 or 1,000 nM) were added to 96-well plates (Equilibrium Dialyzer MW10K; Harvard Apparatus), followed by equilibrium dialysis (22 h at 37 °C). A certain amount of methanol solution containing sulfaphenazole was added as an internal standard to the separated filtrate, brain homogenate fractions and pre-dialyzed samples, and centrifuged ($1,700 \times g$, 10 min). The supernatant fractions were applied to liquid

chromatography with tandem mass spectrometry (LC–MS/MS) to measure the DCZ concentration. The average fraction of unbound brain tissue was calculated for each concentration, as reported in a previous publication[35].

Drug administration. DCZ (HY-42110, MedChemExpress or synthesized in-house, see below) was dissolved in 1–2% dimethyl sulfoxide (DMSO) in saline to a final volume of 0.1 ml per kg. CNO (Toronto Research) was dissolved in 2.5% DMSO in saline to a final volume of 0.1 ml per kg. C21 (Tocris) was dissolved in 2% DMSO in distilled water to a final volume of 0.1 ml per kg. For plasma/CSF analysis, a 23-gauge catheter was placed in the saphenous vein or the spinal canal for acute sampling while the monkey was under ketamine and xylazine anesthesia. DCZ (100 μg per kg) was administered at a rate of 0.2 ml s^{-1} intravenously via catheter. For PET blocking and occupancy studies, DCZ (10, 30, 100 or 1,000 μg per kg), CNO solution (100, 300, 1,000, 3,000 or 10,000 μg per kg) or C21 (300, 1,000 or 6,000 μg per kg) was administered intravenously via a saphenous vein catheter 1–15 min before PET imaging. For the FDG–PET study, DCZ (1, 3 or 100 μg per kg) solution or vehicle was administered intravenously 1 min before PET imaging. Fresh solutions were prepared on the day of usage.

Synthesis of DCZ. 1-Methylpiperazine (0.33 ml, 2.97 mmol) was added to a solution of 11-chloro-5H-dibenzo[b,e][1,4]diazepine (0.22 g, 0.96 mmol)[12] in toluene (5 ml). The resulting solution was refluxed for 2 h. After cooling down to room temperature, the reaction was concentrated. The resulting residue was purified by silica gel flash column chromatography with 0–10% methanol in dichloromethane to give the desired product (0.20 g, yield 70%). ^{1}H NMR (800 MHz, CD3OD) δ: 7.69–7.64 (m, 2H), 7.41 (d, J = 7.9 Hz, 1H), 7.33–7.29 (m, 2H), 7.27 (t, J = 7.6 Hz, 1H), 7.19–7.13 (m, 2H), 4.40–3.80 (br, 4H), 3.80–3.50 (br, 4H), 3.06 (s, 3H). HRMS calculated for $C_{18}H_{21}N_4$: 293.1761; found: 293.1720 [M + H]$^+$.

Radiosynthesis. [^{11}C]DCZ was produced as follows. An automated multipurpose synthesizer developed in-house was used for the radiosynthesis. The cyclotron-produced [^{11}C]CO_2 was converted to [^{11}C]CH_3I, which was distilled and sent through a silver trifluoromethanesulfonate glass tube under N_2 gas flow to yield [^{11}C]methyl trifluoromethanesulfonate ([^{11}C]CH_3OTf). [^{11}C]CH_3OTf was then introduced to a reaction vial containing desmethyl precursor (C21, 0.2 mg) in dichloromethane (0.3 ml) under room temperature. The reaction mixture was kept at room temperature for 5 min. high-performance LC (HPLC) purification was completed on an X-Bridge C18 column (10 mm inner diameter × 250 mm, Waters) using CH_3CN/H_2O/Et$_3$N (acetonitrile/water/triethylamine) (40/60/0.1%) at 5.0 ml min^{-1}. The radioactive fraction corresponding to [^{11}C]DCZ (t_R: 9.5 min) was collected and formulated to obtain an injectable solution. Synthetic time was about 40 min from the end of bombardment with the averaged radiochemical yield (decay-corrected) of 76.2% based on [^{11}C]CO_2 (N = 16). Radiochemical purity was assayed by analytical HPLC (column: Capcell Pak C18 UG120 S5, 4.6-mm inner diameter, 150-mm length; Shiseido) ultraviolet detector at 254 nm; mobile phase of CH_3CN/H_2O (40/60) (Et$_3$N 0.1%). Radiochemical purity and molar activity of [^{11}C]DCZ were >98% and 130 ± 45 GBq μmol^{-1} (N = 16), respectively.

[^{11}C]clozapine was radiosynthesized from desmethylclozapine by ^{11}C-methylation using ^{11}C-methyl triflate based on a previously described protocol[36], and its radiochemical purity and specific radioactivity at the end of synthesis exceeded 95% and 37 GBq μmol^{-1}, respectively. [^{18}F]FDG was purchased from Nihon Medi-Physics.

PET imaging. PET scans were performed using a microPET Focus 220 scanner (Siemens Medical Solutions USA). Anesthesia was performed as follows: a mouse was anesthetized with 1–3% isoflurane and a monkey was immobilized by i.m. injection of ketamine (5–10 mg per kg) and xylazine (0.2–0.5 mg per kg) and then maintained in an anesthetized condition with isoflurane (1–3%) during all PET procedures. Transmission scans were performed for about 20 min with a Ge-68 source for monkey scans. Emission scans were acquired in three-dimensional (3D) list mode with an energy window of 350–750 keV after i.v. bolus injection of [^{11}C]DCZ (31.8–46.4 MBq for mice and 276.9–386.9 MBq for monkeys), [^{11}C]clozapine (287.4–353.8 MBq), [^{11}C]CNO (354.6 MBq) or [^{18}F]FDG (157.6–358.5 MBq). The actual injected dose depended on the specific radioactivity and the weight of the subjects (for example, <0.8 μg per kg for monkey 209). Emission data acquisition lasted 90 min for [^{11}C]DCZ, [^{11}C]clozapine and [^{11}C]CNO scans and 120 min for [^{18}F]FDG scans. All list-mode data were sorted into 3D sinograms, which were then Fourier-rebinned into two-dimensional sinograms (frames × minutes: 5 × 1, 5 × 2, 5 × 3 and 12 × 5 for [^{11}C]DCZ and [^{11}C]clozapine, 24 × 5 for [^{18}F]FDG). Images were thereafter reconstructed with filtered back-projection using a Hanning filter cut-off at a Nyquist frequency (0.5 mm^{-1}). SUVs were calculated using PMOD image analysis software as the regional concentration of radioactivity averaged across the specific time window after injection of the radioligand. Volumes of interest (VOIs) were placed using PMOD image analysis software with reference to the MR image of individual monkeys or the mouse brain template generated as previously described[15]. To obtain accurate registrations between PET and MR images, the rigid matching function of PMOD (PFUS) was used. For this PET–MR registration, maximum errors in translation and

rotation of human brain data were 1.67 mm and 0.6°, respectively[37], despite the fact that no data were available for monkey brains. In addition to the registration error, there should be spatial limitation of PET imaging of the 'positive region' due to the signal spread from the source. Based on our in vivo and in vitro cross reference, we approximated that the limitation was <2 mm. In FDG studies of hM3Dq-expressing monkeys, the VOI for the hM3Dq-positive region was defined as the area where the BP_{ND} value of [^{11}C]DCZ was higher than 1.0, while that of the control region was placed at the corresponding contralateral side.

Two-photon laser-scanning microscopy. Awake mice were placed on a custom-made apparatus, and real-time imaging was conducted by two-photon microscopy (TCS-SP5 MP, Leica Microsystems) with an excitation wavelength of 900 nm. An emission signal was separated by a beam splitter (560/10 nm) and simultaneously detected with a band-pass filter for SR101 (610/75 nm) and GCaMP6 (525/50 nm). A single image plane consisted of 512 × 512 pixels, and the in-plane pixel size was 0.9 μm × 0.9 μm. The methods for functional imaging using two-photon microscopy have been reported in detail[38]. Briefly, continuous image capturing was conducted for neurons on the surface over the barrel cortex at a rate of 0.25 s per frame for 60 s with a 512 × 512 pixel field of view. The percentage change in green fluorescence of neurons was manually measured offline with LAS AF software (Leica Microsystems). Sensory-evoked neuronal excitation was examined by means of whisker stimulation as previously reported[38]. Air puff stimulations (15 p.s.i., 50-ms pulse width, 10 s duration, 10 Hz) were given to whiskers on the contralateral side of scanning 4 times in a day.

Electrophysiology. Electrophysiological recordings were performed on one monkey while seated in a monkey chair with its head fixed via a headpost, and maintained under an anesthetized condition with i.v. infusion of propofol (20 mg per kg per h). LFPs were recorded using a multicontact linear probe with 12 recording contacts separated by 150 μm (Axial Array, FHC). The probe was inserted into the brain with a hydraulic micromanipulator (MO-97A, Narishige) guided with a stainless steel tube and an implanted recording chamber system (Crist Instruments). Chamber grids were either purchased from Crist Instruments or custom-made with a 3D printer (Object260 Connex3, Stratasys). For every recording session, the monkey was CT scanned before the recording probe was removed. The electrode location relative to hM3Dq expression was confirmed by aligning the CT image with the pre-acquired PET image on PMOD. The probe was connected to a multichannel acquisition system (System 3, Tucker-Davis Technologies) running on a Windows PC. For LFPs, the signals were band-pass filtered between 1.5 Hz and 500 Hz, and sampled at 3 kHz. LFP signals were further analyzed only when multiunit waveforms were qualitatively observed in a high frequency band (that is, 400 Hz to 5 kHz) at the corresponding recording sites. The spectral component of the LFP signal was analyzed with Matlab (MathWorks). The spectral power of each frequency was computed using a short-time fast Fourier transform algorithm within a 60-s window sliding in 30-s steps. The change in the gamma band power (40 Hz) and its change relative to that in a 3- or 10-min pre-injection period was quantified. The spectrogram was smoothed with a Hanning window with 4.3-min half-maximum width for display reasons.

Behavioral testing. Monkeys 226, 229 and 245 were tested with a spatial delayed-response task (Fig. 7c). The protocol was based on previous studies using the Wisconsin general testing apparatus[39,40]. Behavioral testing was conducted in a sound-attenuated room. Monkeys were seated in a monkey chair from which they could reach out one hand and take food to their mouths. A wooden table with two food wells was placed in front of the monkeys, and a screen was placed between the monkeys and the table. First, a piece of food reward (raisin or half peanut) was placed in one of the two food wells, and then both wells were covered with wooden plates. Then, the screen was placed for 0.5, 5 or 10 s, which served as delay periods (0.5-s delay was not introduced for non-DREADD monkeys). The position of the baited well (left or right) was pseudorandomly determined. After the delay period, the screen was removed and the monkeys were allowed to select either food well to get the food. The monkeys were allowed to take the food if they reached to the correct food well and removed the cover plate. The inter-trial interval was set at 10–15 s. A daily session lasted about 1 h and consisted of 3–4 blocks of 20–30 trials, which were interleaved by a 5-min rest period. The behavioral testing began immediately or 1 h after an i.m. administration of either vehicle (2% DMSO in saline) or DCZ (100 μg per kg), and was conducted on the next day (24 h later) of the DCZ administration. One of the monkeys injected with AAV-hM4Di in the bilateral PFC (monkey 229) was also tested in a non-memory control task, which was almost the same as the delayed response task except that the screen was not placed during the delay period and that the 0.5-s delay was not introduced.

Three monkeys without AAV injections (non-DREADD; monkeys 224, 228 and 230) were tested with a reward-size task (Supplementary Fig. 6a) using the same protocol as applied in a previous study[41]. The behavioral testing began 10 min after an i.m. administration of either vehicle (2% DMSO in saline) or DCZ (100 μg per kg).

Histology and immunostaining. The monkeys were deeply anesthetized with an overdose of sodium pentobarbital (80 mg per kg, i.v.) and transcardially perfused

with saline at 4 °C, followed by 4% paraformaldehyde in 0.1 M PBS, pH 7.4. The brains were removed from the skull, post-fixed in the same fresh fixative overnight, saturated with 30% sucrose in phosphate buffer (PB) at 4 °C, and then cut serially into 50-μm-thick sections on a freezing microtome. For visualization of immunoreactive signals of hM4Di, a series of every sixth section was immersed in 1% skim milk for 1 h at room temperature and incubated overnight at 4 °C with rabbit anti-M4 polyclonal antibody (1:200; H-175, Millipore) in PBS containing 0.1% Triton X-100 and 1% normal donkey serum for 2 days at 4 °C. The sections were then incubated in the same fresh medium containing biotinylated donkey anti-rabbit IgG antibody (1:1,000; Jackson ImmunoResearch) for 2 h at room temperature, followed by avidin–biotin–peroxidase complex (ABC Elite, Vector Laboratories) for 2 h at room temperature. For visualization of the antigen, the sections were reacted in 0.05 M Tris-HCl buffer (pH 7.6) containing 0.04% diaminobenzidine (DAB), 0.04% NiCl₂ and 0.003% H₂O₂. The sections were mounted on gelatin-coated glass slides, air dried and cover-slipped. A part of other sections was Nissl stained with 1% Cresyl violet. The same protocol was used for visualization of immunoreactive signals of hM3Dq with rabbit anti-M3 polyclonal antibody (1:200; HPA024106, Atlas Antibodies).

The mice were deeply anesthetized with sodium pentobarbital and then transcardially perfused with PBS. Brain tissues were removed and fixed with 4% paraformaldehyde in PB overnight, followed by cryoprotection with 30% sucrose in PB. Frozen sections (10-μm thick) were generated using a cryostat (HM560; Carl Zeiss). Visualization of immunoreactive signals of hM4Di was performed using an anti-M4 antibody (H-175) and fluorophore-conjugated secondary antibodies (Invitrogen) as previously described[15].

Images of sections were digitally captured using an optical microscope equipped with a high-grade charge-coupled device camera (Biorevo, Keyence).

PK analysis. Four monkeys and 15 mice were used to assess the concentration of DCZ and its metabolites in plasma, CSF or brain. In monkeys, blood and CSF were collected at 15, 30, 45, 60, 75, 90, 105 and 120 min after DCZ administration (100 μg per kg, i.v. or i.m.) under ketamine and xylazine anesthesia. In mice, after i.p. injection of DCZ (100 μg per kg), blood and brain samples were collected at 5, 30, 60, 120 min or 24 h, and CSF was collected at 30 and 120 min. Mouse blood was collected by heparinized syringes via the heart under isoflurane anesthesia followed by centrifugation at $10,000 \times g$ for 5 min to obtain plasma samples, and brains were removed and frozen by liquid nitrogen immediately after blood collection. All samples were stored at −80 °C until analysis.

The protocols for sample pretreatment of CSF and plasma have been previously described[6]. Mouse brains were homogenized in 2-brain-weight water. An acetonitrile solution (0.8 ml) containing granisetron (0.5 ng ml⁻¹) as an internal standard was added to the brain homogenate (0.2 ml), followed by centrifugation at $10,600 \times g$ for 2 min at 4 °C. The supernatant was collected and filtered through a solid-phase extraction column (Phree, Shimadzu). The filtrate was dried under nitrogen gas at 40 °C and redissolved in 5% acetonitrile (0.2 ml) followed by sonication for 30 s and centrifugation ($500 \times g$) for 2 min. The supernatant was filtered through a solid-phase extraction column again before its application to LC–MS/MS.

Quantification of C21, DCZ and DCZ-N-oxide was performed by multiple reaction monitoring using a Shimadzu UHPLC LC-30AD system (Shimadzu) coupled to a tandem MS AB Sciex Qtrap 6500 system (AB Sciex). The following multiple reaction monitoring transitions (Q1/Q3) were used to monitor each compound: C21 (279.0/193.0), DCZ (293.0/236.0), DCZ-N-oxide (309.0/192.9) and granisetron (313.2/138.1). Other protocols have been previously described[6].

Statistical analyses. *In vitro assays.* All data were analyzed using GraphPad Prism 7. Inhibition binding data were analyzed according to a one-site binding model, and the equilibrium dissociation constant (K_d) values of unlabeled ligands were calculated by constraining the radioligand K_d values to the values estimated from saturation binding assays. Concentration–response curves were fitted to a three-parameter logistic equation. All affinity and potency values were estimated as logarithms.

PET imaging. To estimate the specific binding of [¹¹C]DCZ, the regional binding potential relative to nondisplaceable radioligand (BP_{ND}) was calculated using PMOD with an original multilinear reference tissue model (MRTMo)[42] as described by the following equation:

$$\frac{\int_0^T C(t)dt}{C(T)} = \frac{V}{V'}\frac{\int_0^T C'(t)dt}{C(T)} + \frac{V}{V'k_2'}\frac{C'(T)}{C(T)} + b \qquad (1)$$

where $C(t)$ and $C'(t)$ are the regional or voxel time–radioactivity concentrations in the tissue and reference regions, respectively (kBq ml⁻¹), V and V' are the corresponding total distribution volumes (ml/ml), k_2' (min⁻¹) is the clearance rate constant from the reference region to plasma, and b is the intercept term, which becomes the constant for $T > t^*$. In this study, t^* was determined as 2 min for the mouse studies and 15 min for the monkey studies. Equation 1 allows estimation of three parameters, $\beta_1 = V/V'$, $\beta_2 = V/(V'k_2')$ and $\beta_3 = b$ by multilinear regression analysis for $T > t^*$. Assuming that the nondisplaceable distribution volumes in

tissue and reference regions are identical, BP_{ND} ($BP_{ND} = V/V' - 1$) is calculated from the first regression coefficient as $BP_{ND} = (\beta_1 - 1)$.

Estimates of fractional occupancy (Occ) were calculated using the following equation:

$$\text{Occ} = \left(^{\text{hM4Di}}BP_{BL} - ^{\text{hM4Di}}BP_{PT}\right)/\left(^{\text{hM4Di}}BP_{BL} - ^{\text{CON}}BP_{BL}\right) \qquad (2)$$

where $^{\text{hM4Di}}BP_{BL}$ and $^{\text{CON}}BP_{BL}$ indicate BP_{ND} at the hM4Di-expressing putaminal region and control putamen under baseline conditions, respectively, while $^{\text{hM4Di}}BP_{PT}$ indicates BP_{ND} at the hM4Di-expressing putaminal region under the pretreatment condition. The relationship between occupancy and agonist dose ($D_{agonist}$) was modeled using the Hill equation as follows:

$$\text{Occ} = D_{agonist}^n / \left(D_{agonist}^n + ED_{50}^n\right) \qquad (3)$$

where ED_{50} and n indicate the agonist dose achieving 50% occupancy and the Hill coefficient, respectively.

For FDG–PET analysis, dynamic SUV images were motion corrected and then were averaged between 30 and 60 min after injection of the radioligand. Voxel-wise statistical analyses were performed using SPM12 software (Wellcome Department of Cognitive Neurology, London, UK; www.fil.ion.ucl.ac.uk) and Matlab R2016a (MathWorks). We used a total of 12 scans including vehicle and DCZ 3 μg per kg pretreatment conditions to detect the metabolic change by hM3Dq activation and a total of 12 scans including vehicle and DCZ 100 μg per kg pretreatment conditions to examine the effect of off-target actions in the non-DREADD monkeys. The averaged SUV images were spatially normalized into a standard template brain MR image[43] after co-registration of individual MR images. The resulting images were smoothed with a 2.6-mm Gaussian filter and then extracted using a brain mask. The SUVs for each scan were corrected using grand mean scaling and by analysis of covariance for global normalization. Subsequently, one-way ANOVA within subject was applied. The statistical threshold was set at uncorrected $P < 0.001$ ($F_{(1,8)} > 20.25$) and an extent of 100 contiguous voxels per cluster. For the VOI-based analysis, we used a total of 17 scans from hM3Dq-expressing monkeys including vehicle and 1 and 3 μg per kg DCZ pretreatment conditions, and a total of 16 scans from non-DREADD monkeys including vehicle and 1 and 100 μg per kg DCZ pretreatment conditions. The SUVs were obtained using PMOD and then were normalized by whole-brain value. Paired t-test was used to detect the metabolic change by hM3Dq activation in each condition. To examine the dose-dependency or off-target actions, one-way ANOVA followed by post hoc Tukey–Kramer test was performed.

Neuronal activity. Time-dependent changes in fluorescence signals and LFP power were analyzed according to a one-phase exponential association model using GraphPad Prism 7. Repeated-measures ANOVA followed by post hoc Dunnett test was used to examine differences between baseline and drug-evoked mean neural signals. The signals were displayed after normalization to the baseline levels, but statistical tests were conducted on the original data.

To examine the long-term effect of hM3Dq activation on normal neuronal responsiveness, the fluorescence signal change within 0.2–10.2 s after whisker stimulation onset was averaged across 4 trials and compared using pairwise t-test. DCZ-induced fluorescence signal changes at 10 min after the first and second DCZ administrations were compared by pairwise t-test. The second DCZ administration was applied 24 h after the first.

Behavioral testing. To examine the effect of DCZ on the performance of the delayed-response task, behavioral measurement (correct rates) was subjected to two-way ANOVA (treatment × delay) and post hoc t-test with Bonferroni correction using GraphPad Prism 7. To examine whether the performance was recovered at 24 h after DCZ administration, the same procedures were conducted between DCZ and post-DCZ, and vehicle and post-DCZ sessions. To examine the effect of DCZ treatment on the behavior in test time, the data of 5- and 10-s delays were pooled and then compared between treatment conditions by t-test. To examine the effect of DCZ on the performance of the reward-size task, reaction times and error rates were subjected to two-way ANOVA (treatment × reward size). The total correct trial number for each session was subjected to two-way ANOVA (treatment × subject). For each analysis, effect size eta-squared (η^2) was calculated using R.

General data collection and statistical statements. Data collection and analyses were not performed blinded to the conditions of the experiments, except for the in vitro studies, which were blinded. For in vivo experiments, the order of drug administration (for example, DCZ or vehicle) was pseudorandom and shuffled across animals. No samples were excluded from the analysis. Statistical tests included parametric and nonparametric methods. All statistical tests were two-sided unless specifically stated otherwise. In some statistical tests, data distributions were assumed to be normal and/or with equal variances, but this was not formally tested. No statistical methods were used to predetermine sample sizes, but our sample sizes were similar to those reported in previous publications (for example, see refs. [5–8,10,30]).

Data availability

The data that support the findings of this study are available from the corresponding authors upon reasonable request.

Code availability

The code to generate the results and the figures of this study are available from the corresponding authors upon reasonable request.

References

33. Tomita, Y. et al. Long-term in vivo investigation of mouse cerebral microcirculation by fluorescence confocal microscopy in the area of focal ischemia. *J. Cereb. Blood Flow Metab.* **25**, 858–867 (2005).
34. Tajima, Y. et al. Changes in cortical microvasculature during misery perfusion measured by two-photon laser scanning microscopy. *J. Cereb. Blood Flow Metab.* **34**, 1363–1372 (2014).
35. Fridén, M. et al. Measurement of unbound drug exposure in brain: modeling of pH partitioning explains diverging results between the brain slice and brain homogenate methods. *Drug Metab. Dispos.* **39**, 353–362 (2011).
36. Bender, D., Holschbach, M. & Stöcklin, G. Synthesis of n.c.a. carbon-11 labelled clozapine and its major metabolite clozapine-*N*-oxide and comparison of their biodistribution in mice. *Nucl. Med. Biol.* **21**, 921–925 (1994).
37. Kiebel, S. J., Ashburner, J., Poline, J.-B. & Friston, K. J. MRI and PET coregistration—a cross validation of statistical parametric mapping and automated image registration. *NeuroImage* **5**, 271–279 (1997).
38. Takuwa, H. et al. Reproducibility and variance of a stimulation-induced hemodynamic response in barrel cortex of awake behaving mice. *Brain Res.* **1369**, 103–111 (2011).
39. Croxson, P. L., Kyriazis, D. A. & Baxter, M. G. Cholinergic modulation of a specific memory function of prefrontal cortex. *Nat. Neurosci.* **14**, 1510–1512 (2011).
40. Goldman, P. S., Rosvold, E. H. & Mishkin, M. Evidence for behavioral impairment following prefrontal lobectomy in the infant monkey. *J. Comp. Physiol. Psychol.* **70**, 454–463 (1970).
41. Minamimoto, T., La Camera, G. & Richmond, B. J. Measuring and modeling the interaction among reward size, delay to reward, and satiation level on motivation in monkeys. *J. Neurophysiol.* **101**, 437–447 (2008).
42. Ichise, M. et al. Noninvasive quantification of dopamine D2 receptors with iodine-123-IBF SPECT. *J. Nucl. Med.* **37**, 513–520 (1996).
43. McLaren, D. G. et al. A population-average MRI-based atlas collection of the rhesus macaque. *NeuroImage* **45**, 52–59 (2009).

Competing interests

Y.N., N.M., B.J., T.S., M.H. and T.M. are named as inventors on a patent application (PCT/JP2019/024834; status: patent pending) claiming subject matter related to the results described in this paper. The remaining authors declare no competing interests.

Additional information

Supplementary information is available for this paper at https://doi.org/10.1038/s41593-020-0661-3.

Correspondence and requests for materials should be addressed to B.L.R. or T.M.

Peer review information *Nature Neuroscience* thanks Mikhail Shapiro and the other, anonymous, reviewer(s) for their contribution to the peer review of this work.

Reprints and permissions information is available at www.nature.com/reprints.